Radially excited $U(1)$ gauged Q-balls

A. Yu. Loginov[1,*] and V. V. Gauzshtein[2]

[1]*Tomsk State University of Control Systems and Radioelectronics, 634050 Tomsk, Russia*
[2]*Tomsk Polytechnic University, 634050 Tomsk, Russia*

Radially excited $U(1)$ gauged Q-balls are studied using both analytical and numerical methods. Unlike the nongauged case, there exists only a finite number of radially excited gauged Q-balls at given values of the model's parameters. Similarly to the unexcited gauged Q-ball, the radially excited one cannot possess the Noether charge exceeding some limiting value. This limiting Noether charge decreases with an increase in the radial excitation of the gauged Q-ball. For nth radial excitation, there is a maximum allowable value of the gauge coupling constant, and the existence of the nth radially excited gauged Q-ball becomes impossible if the gauge coupling constant exceeds this limiting value. Similarly to the limiting Noether charge, the limiting gauge coupling constant decreases with an increase in the radial excitation. At a fixed Noether charge, the energy of the gauged Q-ball increases with an increase in the radial excitation, and thus the radially excited gauged Q-ball is unstable against transit into a less excited or unexcited one.

I. INTRODUCTION

In the framework of field theory, solitons are spatially localized, nonspreading solutions to field equations possessing finite energy. Solitons play an important role in high-energy physics, condensed matter physics, cosmology, and hydrodynamics. They can be divided into two main groups: topological solitons and nontopological solitons. The existence and stability of topological solitons result from the topological nontriviality of their field configurations [1]. This nontriviality means that a topological soliton cannot be smoothly and continuously deformed into the vacuum field configuration, which is topologically trivial. Hence, there exists an infinite potential barrier between the topological soliton and the vacuum state, and the soliton cannot decay into a field configuration in the functional neighborhood of the topologically trivial vacuum.

In contrast, the field configurations of nontopological solitons are topologically trivial, and the existence of nontopological solitons is therefore due to the dynamics of corresponding field models [2]. In particular, nontopological solitons exist in field models that possess global symmetries (which may be both Abelian and non-Abelian) [3–7] and have interaction potentials that meet certain

*a.yu.loginov@tusur.ru

conditions [2,8]. The basic property of a nontopological soliton is that it is the extremum (minimum or saddle point) of the energy functional at a fixed value of the Noether charge corresponding to the global symmetry group generator of the field model. This feature of nontopological solitons results in the characteristic time dependence $\propto \exp(-i\omega t)$ of their fields. The time dependence of the soliton's field allows the severe restrictions of Derrick's theorem [9] to be avoided, meaning that nontopological solitons composed of scalar fields can exist in space-time with an arbitrary number of spatial dimensions.

The simplest of nontopological solitons is the Q-ball [5], a coherent state of a self-interacting complex scalar field. Q-balls exist in models of complex scalar fields possessing $U(1)$ global symmetry and certain self-interaction potentials. The characteristic feature of nontopological solitons in general and of Q-balls in particular is the presence of an infinite number of radially excited states in addition to the basic unexcited state [4,10–12]. The basic and radially excited states of Q-balls are spherically symmetric. The profile function of the basic unexcited state of a Q-ball has no nodes for any finite radius, whereas the nth radially excited state of a Q-ball has exactly n nodes at finite radii.

When the $U(1)$ symmetry of the model is global, the Noether charge of the Q-ball corresponds to the particle number. However, the global $U(1)$ symmetry can be gauged by means of the Abelian gauge field, which interacts minimally with the model's complex scalar field. As in the case of global $U(1)$ symmetry, the $U(1)$ gauged models of complex self-interacting scalar fields admit the existence of Q-balls [13–24]. These gauged Q-balls are electrically charged objects, and thus possess a long-range

electric field. The electric charge of gauged Q-balls is the product of the Noether charge and the gauge coupling constant, which defines the interaction strength between the gauge field and the complex scalar field. The properties of gauged Q-balls differ significantly from those of non-gauged ones. In particular, the Noether (electric) charge and the energy of gauged Q-balls cannot be arbitrarily large [14,24], provided that the second derivative of the self-interaction potential $d^2V(|\phi|)/d|\phi|^2$ is finite at the origin [20]. A gauged Q-ball also cannot exist if the gauge coupling constant exceeds some maximum value [14], which depends on the other parameters of the model.

As in the nongauged case, there exist radially excited gauged Q-balls. These also cannot possess an arbitrarily large electric charge and can exist only if the gauge coupling constant does not exceed some limiting value; both the maximum possible Noether charge and the maximum possible gauge coupling constant decrease with an increase in the radial excitation of a gauged Q-ball. Furthermore, there is only a finite number of radially excited gauged Q-balls for given values of the gauge coupling constant and the other parameters of the model. In this paper, we study radially excited gauged Q-balls from both an analytical and numerical perspective. We ascertain the basic properties of these objects and discuss related issues.

The paper is structured as follows. In Sec. II, we describe briefly the Lagrangian, the symmetries, and the field equations of the model under consideration. In Sec. III, the general properties of the gauged Q-balls are considered and discussed. In Sec. IV, we present numerical results for radially excited gauged Q-balls. Some numerical results relating to unexcited gauged Q-balls are also included in Sec. IV for completeness. In the final section, we briefly summarize the results obtained in this work. Three Appendixes are also included. In Appendix A, we show that the gauged Q-ball's fields do not depend on time in the unitary gauge and establish the basic relation between the energy and the Noether charge of the gauged Q-ball. In Appendix B, we discuss the reason for the existence of the maximum possible electric charge for gauged Q-balls. In Appendix C, we ascertain the reason for the existence of the inflection point in the curve describing the dependence of the energy of the gauged Q-ball on the Noether charge.

Throughout this paper, we use the natural units $c = 1$, $\hbar = 1$.

II. LAGRANGIAN AND FIELD EQUATIONS OF THE MODEL

The gauge model we are interested in has the Lagrangian density

$$\mathcal{L} = -\frac{1}{4}F_{\mu\nu}F^{\mu\nu} + (D_\mu\phi)^*D^\mu\phi - V(|\phi|). \tag{1}$$

This model describes the self-interacting complex scalar field ϕ minimally interacting with the Abelian gauge field A_μ through the covariant derivative

$$D_\mu\phi = \partial_\mu\phi + ieA_\mu\phi. \tag{2}$$

The local gauge transformations

$$\phi(x) \to \phi'(x) = \exp\left(-ie\Lambda(x)\right)\phi(x),$$
$$A_\mu(x) \to A'_\mu(x) = A_\mu(x) + \partial_\mu\Lambda(x) \tag{3}$$

leave invariant the Lagrangian density (1). A special case of Eq. (3) is the global phase transformations $\phi(x) \to \phi'(x) = \exp\left(-i\alpha\right)\phi(x)$. The invariance of the Lagrangian density (1) under these global phase transformations leads to the conserved Noether current of the model

$$j_N^\nu = i[\phi^*D^\nu\phi - (D^\nu\phi)^*\phi]. \tag{4}$$

The self-interaction of the complex scalar field is described by the six-order potential

$$V(|\phi|) = m^2|\phi|^2 - \frac{g}{2}|\phi|^4 + \frac{h}{3}|\phi|^6, \tag{5}$$

where the self-interaction coupling constants g and h are assumed to be positive. We assume that the potential $V(|\phi|)$ has a global minimum at $\phi = 0$ and thus there is no spontaneously broken gauge symmetry. For this to hold, the parameters of the potential in Eq. (5) must satisfy the inequality $3g^2 < 16hm^2$.

By varying the action $S = \int \mathcal{L}d^3xdt$ in the corresponding fields, we obtain the field equations of the model,

$$D_\mu D^\mu\phi + m^2\phi - g|\phi|^2\phi + h|\phi|^4\phi = 0, \tag{6}$$

$$\partial_\mu F^{\mu\nu} = j^\nu, \tag{7}$$

where the electromagnetic current density $j^\nu = ej_N^\nu$. Later on, we shall also need the expression for the energy-momentum tensor for a field configuration of the model,

$$T_{\mu\nu} = -F_{\mu\lambda}F_\nu{}^\lambda + \frac{1}{4}\eta_{\mu\nu}F_{\lambda\rho}F^{\lambda\rho} + (D_\mu\phi)^*D_\nu\phi$$
$$+ (D_\nu\phi)^*D_\mu\phi - \eta_{\mu\nu}((D_\mu\phi)^*D^\mu\phi - V(|\phi|)), \tag{8}$$

where the metric tensor $\eta_{\mu\nu} = \text{diag}(+1, -1, -1, -1)$.

III. SOME PROPERTIES OF GAUGED Q-BALLS

By definition, the Q-ball field configuration is an extremum of the energy functional $E = \int T_{00}d^3x$ at a fixed value of the Noether charge $Q_N = \int j_N^0 d^3x$. Thus, the Q-ball field configuration is a conditional extremum of the energy functional. According to Lagrange's method of

multipliers, the Q-ball is an unconditional extremum of the functional $F = E - \lambda Q_N$, where λ is the Lagrange multiplier. Using Lagrange's method of multipliers and the Hamilton field equations, we show in Appendix A that the Q-ball field configuration does not depend on time in the unitary gauge $\text{Im}(\phi) = 0$. Next, we assume that in the unitary gauge the Q-ball field configuration is spherically symmetric. The spherical symmetry, time independence, and regularity of the Q-ball field configuration lead to the vanishing of the spatial components of the electromagnetic current density j^k in the unitary gauge (and consequently in any other gauge, since the electromagnetic current density is gauge invariant). Since in the unitary gauge $j^k = -2e^2 A^k \text{Re}(\phi)$, the spatial components A^k of the electromagnetic potential also vanish. Thus, we have the ansatz for the Q-ball fields in the unitary gauge

$$\phi(\mathbf{x}, t) = \frac{f(r)}{\sqrt{2}}, \qquad A^\mu(\mathbf{x}, t) = \eta^{\mu 0} A_0(r), \qquad (9)$$

where $f(r)$ and $A_0(r)$ are the real ansatz functions depending on the radial variable r.

Since the Q-ball is an unconditional extremum of the functional $F = E - \lambda Q_N$, the first variation of F vanishes in the neighborhood of the Q-ball solution

$$\delta F = \delta E - \lambda \delta Q_N = 0. \qquad (10)$$

Equation (10) holds for arbitrary variations in fields in the neighborhood of the Q-ball solution, including those that change the Q-ball solution to an infinitesimally close one. It follows that the energy of the gauged Q-ball satisfies the important relation

$$\frac{dE}{dQ_N} = \lambda, \qquad (11)$$

where the Lagrange multiplier λ is a function of the Noether charge Q_N. Since the Q-ball's energy and the Noether charge are gauge invariant, the Lagrange multiplier λ is also gauge invariant. It is shown in Appendix A that in the unitary gauge the Lagrange multiplier λ is expressed in terms of the limiting value of the electromagnetic potential at spatial infinity:

$$\lambda = -e \lim_{r \to \infty} A_0(r) \equiv \Omega_\infty. \qquad (12)$$

Substituting ansatz (9) into field equations (6) and (7), we obtain a system of nonlinear differential equations for the ansatz functions $f(r)$ and $\Omega(r) = -eA_0(r)$:

$$f''(r) + \frac{2}{r} f'(r) - (m^2 - \Omega(r)^2) f(r)$$
$$+ \frac{g}{2} f(r)^3 - \frac{h}{4} f(r)^5 = 0, \qquad (13)$$

$$\Omega''(r) + \frac{2}{r} \Omega'(r) - e^2 \Omega(r) f(r)^2 = 0. \qquad (14)$$

The regularity of the Q-ball field configuration and the finiteness of the Q-ball's energy lead to the boundary conditions for the ansatz functions:

$$f'(0) = 0, \qquad f(r) \xrightarrow[r \to \infty]{} 0,$$
$$\Omega'(0) = 0, \qquad \Omega(r) \xrightarrow[r \to \infty]{} \Omega_\infty. \qquad (15)$$

The general properties of the electromagnetic potential A_0 of the gauged Q-ball were established in Ref. [14]. In terms of the ansatz function $\Omega(r)$, these properties are formulated as

$$0 < \Omega(r_1) < \Omega(r_2) < \Omega_\infty \quad \text{if } \Omega_\infty > 0, \qquad (16a)$$

$$0 > \Omega(r_1) > \Omega(r_2) > \Omega_\infty \quad \text{if } \Omega_\infty < 0, \qquad (16b)$$

where it is supposed that $r_1 < r_2$. We see that $\Omega(r)$ is a positive and increasing (negative and decreasing) function of r if its limiting value Ω_∞ is positive (negative).

The Lagrangian (1) is invariant under the charge conjugation: $A_\mu \to -A_\mu$, $\phi \to \phi^*$. This invariance of the Lagrangian results in the invariance of Eqs. (13) and (14) under the change of sign $\Omega \to -\Omega$. Furthermore, the invariance of the Lagrangian (1) under the other discrete transformation $\phi \to -\phi$ [which is a particular case of the phase transformation $\phi \to \exp(-i\alpha)\phi$] leads to the invariance of Eqs. (13) and (14) under the change of sign $f \to -f$.

We now consider the asymptotic behavior of the gauged Q-ball solution at small and large r. Substituting the power expansions for the ansatz functions into Eqs. (13) and (14), we obtain the asymptotic form of the Q-ball solution at small r,

$$f(r) = f_0 + \frac{f_2}{2!} r^2 + O(r^2), \qquad (17a)$$

$$\Omega(r) = \Omega_0 + \frac{\Omega_2}{2!} r^2 + O(r^2), \qquad (17b)$$

where the next-to-leading coefficients are expressed in terms of f_0 and Ω_0,

$$f_2 = \frac{1}{3} \left((\Omega_0^2 - m^2) f_0 - \frac{g}{2} f_0^3 + \frac{h}{4} f_0^5 \right), \qquad (18a)$$

$$\Omega_2 = \frac{1}{3} e^2 f_0^2 \Omega_0. \qquad (18b)$$

At large r, Eq. (14) can be linearized, and we obtain the asymptotic form of $\Omega(r)$ as $r \to \infty$,

$$\Omega(r) \sim \Omega_\infty - \frac{e}{4\pi}\frac{Q}{r}, \tag{19}$$

where $Q = 4\pi \int_0^\infty j_0(r)r^2 dr$ is the total electric charge of the gauged Q-ball. We see that, due to the long-range character of the electromagnetic interaction, the ansatz function Ω tends rather slowly (approximately r^{-1}) to the limiting value Ω_∞. Because of this, in Eq. (13), the gauge field does not decouple from the scalar field even at large r. This results in the asymptotics [24] for the complex scalar field as $r \to \infty$

$$f(r) \sim f_\infty(\Delta r)^{-(1+\frac{\beta}{2\Delta})} \exp(-\Delta r), \tag{20}$$

where

$$\Delta = (m^2 - \Omega_\infty^2)^{1/2}, \qquad \beta = \frac{e}{2\pi}\Omega_\infty Q, \tag{21}$$

and f_∞ is a constant. We see that the long-range tail of the gauge field leads to a faster decrease in the complex scalar field of the gauged Q-ball at large r in comparison with the nongauged Q-ball for which $f(r) \sim f_\infty(\Delta r)^{-1} \exp(-\Delta r)$. As $|\Omega_\infty| = m$, the exponent $-(1 + 2^{-1}\beta\Delta^{-1})$ of the pre-exponential factor diverges, and Eq. (20) becomes inapplicable. However, it was shown in Ref. [24] that when $|\Omega_\infty| = m$ the scalar field of the gauged Q-ball has the following asymptotics at large r:

$$f(r) \sim f_\infty(mr)^{-3/4} \exp\left(-\sqrt{\frac{2e}{\pi}Qmr}\right). \tag{22}$$

Thus, unlike the nongauged Q-ball, the gauged Q-ball also exists at the limiting point $|\Omega_\infty| = m$ and has a finite energy and Noether charge at this point. At the same time, like the nongauged Q-ball, the gauged Q-ball does not exist when $|\Omega_\infty| > m$ since the asymptotics (20) shows oscillating behavior, leading to an infinite energy and Noether charge for the corresponding field configuration.

The electromagnetic current density and the components of the energy-momentum tensor can also be expressed in terms of the ansatz functions,

$$j_\mu = e\Omega(r)f(r)^2\eta_{\mu 0}, \tag{23}$$

$$T_{00} = \frac{1}{2e^2}\Omega'(r)^2 + \frac{1}{2}f'(r)^2$$
$$+ \frac{1}{2}\Omega(r)^2 f(r)^2 + V(f(r)), \tag{24}$$

$$T_{0k} = 0, \tag{25}$$

$$T_{ij} = \left(\frac{x_i x_j}{r^2} - \frac{1}{3}\delta_{ij}\right)s(r) + \delta_{ij}p(r), \tag{26}$$

where the radially dependent functions

$$s(r) = f'(r)^2 - e^{-2}\Omega'(r)^2 \tag{27}$$

and

$$p(r) = \frac{1}{6e^2}\Omega'(r)^2 - \frac{1}{6}f'(r)^2$$
$$+ \frac{1}{2}\Omega(r)^2 f(r)^2 - V(f(r)) \tag{28}$$

are the shear force and pressure distributions, respectively. From Eqs. (16) and (23), it follows that

$$\text{sign}(j_0(r)) = \text{sign}(\Omega(r)) = \text{sign}(\Omega_\infty), \tag{29}$$

and hence the sign of the electric (Noether) charge coincides with that of the parameter Ω_∞. In contrast, it follows from Eqs. (24)–(28) that the values of the components of the energy-momentum tensor do not depend on the sign of Ω_∞. We conclude that the energy of the gauged Q-ball is an even function of Ω_∞, whereas the electric (Noether) charge is an odd function:

$$E(-\Omega_\infty) = E(\Omega_\infty), \qquad Q(-\Omega_\infty) = -Q(\Omega_\infty). \tag{30}$$

Since the T_{0k} components of the energy-momentum tensor vanish, the angular momentum of the spherically symmetrical gauge Q-ball is equal to zero, as expected. The conservation of the energy-momentum tensor leads to the differential relation between the shear force and the pressure

$$\frac{2}{r}s(r) + \frac{2}{3}s'(r) + p'(r) = 0. \tag{31}$$

Multiplying Eq. (31) by r^3 and integrating by parts over r from zero to infinity, we obtain the Laue condition [25,26] for the pressure distribution

$$\int_0^\infty dr r^2 p(r) = 0. \tag{32}$$

Any solution of field equations (6) and (7) is an extremum of the action $S = \int \mathcal{L}d^3xdt$. In the case of the gauged Q-ball, the Lagrangian density $\mathcal{L}$ does not depend on time, and thus the gauged Q-ball solution is an extremum of the Lagrangian $L = \int \mathcal{L}d^3x$. Next, for the Q-ball solution, the total energy $E = \int T_{00}d^3x$ and the Lagrangian $L = \int \mathcal{L}d^3x$ can be presented as linear combinations of the electrostatic, gradient, kinetic, and potential terms,

$$E = E^{(E)} + E^{(G)} + E^{(T)} + E^{(P)}, \tag{33}$$

$$L = E^{(E)} - E^{(G)} + E^{(T)} - E^{(P)}, \tag{34}$$

where

$$E^{(E)} = 4\pi \int_0^\infty \frac{1}{2e^2} \Omega'(r)^2 r^2 dr, \tag{35a}$$

$$E^{(G)} = 4\pi \int_0^\infty \frac{1}{2} f'(r)^2 r^2 dr, \tag{35b}$$

$$E^{(T)} = 4\pi \int_0^\infty \frac{1}{2} \Omega(r)^2 f(r)^2 r^2 dr, \tag{35c}$$

$$E^{(P)} = 4\pi \int_0^\infty V(f(r)) r^2 dr. \tag{35d}$$

Let us consider the scale transformation of the gauge Q-ball's fields: $f(r) \to f(\kappa r)$, $A_0(r) \to A_0(\kappa r)$. Under this transformation, the terms in Eqs. (35a)–(35d) behave as $E^{(E)} \to \kappa^{-1} E^{(E)}$, $E^{(G)} \to \kappa^{-1} E^{(G)}$, $E^{(T)} \to \kappa^{-3} E^{(T)}$, and $E^{(P)} \to \kappa^{-3} E^{(P)}$, and thus the Lagrangian (34) becomes a function of the scale parameter κ. Since $f(\kappa r)$ and $A_0(\kappa r)$ form the Q-ball solution at $\kappa = 1$, the derivative $dL/d\kappa$ must vanish at this point: $dL/d\kappa|_{\kappa=1} = 0$. The last equation results in the virial relation for the gauged Q-ball

$$E^{(E)} - E^{(G)} + 3(E^{(T)} - E^{(P)}) = 0. \tag{36}$$

It can be easily shown that, given Eqs. (35a)–(35d), the virial relation (36) is equivalent to the Laue condition (32).

The energy of the gauged Q-ball can be presented in several equivalent forms. Integrating the term Ω'^2 in the electrostatic energy density $\Omega'(r)^2/(2e^2)$ by parts, using Eq. (14) (Gauss's law), and taking into account the boundary conditions (15), we obtain the following expression for the electrostatic energy of the gauged Q-ball:

$$E^{(E)} = \frac{1}{2} 4\pi \int_0^\infty (A_0(r) - A_0(\infty)) j_0(r) r^2 dr$$
$$= \frac{1}{2e} 4\pi \int_0^\infty (\Omega_\infty - \Omega(r)) j_0(r) r^2 dr. \tag{37}$$

The kinetic energy (35c) can also be rewritten in terms of the electric charge density:

$$E^{(T)} = -\frac{1}{2} 4\pi \int_0^\infty A_0(r) j_0(r) r^2 dr$$
$$= \frac{1}{2e} 4\pi \int_0^\infty \Omega(r) j_0(r) r^2 dr. \tag{38}$$

Combining Eqs. (33), (35b), (35d), (37), and (38) results in an alternative expression for the energy of the gauged Q-ball,

$$E = \Omega_\infty \frac{Q_N}{2} + 4\pi \int_0^\infty \left(\frac{1}{2} f'(r)^2 + V(f(r)) \right) r^2 dr$$
$$= \Omega_\infty \frac{Q_N}{2} + E^{(G)} + E^{(P)}. \tag{39}$$

Next, Eqs. (33) and (39) lead to the following expression for the Noether charge:

$$Q_N = \frac{2}{\Omega_\infty} (E^{(E)} + E^{(T)}). \tag{40}$$

Finally, using Eqs. (39), (40), and the virial relation (36), we obtain two more expressions for the energy of the gauged Q-ball:

$$E = \Omega_\infty Q_N + \frac{8\pi}{3} \int_0^\infty \left(\frac{1}{2} f'(r)^2 - \frac{1}{2e^2} \Omega'(r)^2 \right) r^2 dr$$
$$= \Omega_\infty Q_N + \frac{2}{3} (E^{(G)} - E^{(E)}) \tag{41}$$

and

$$E = \Omega_\infty Q_N + 8\pi \int_0^\infty \left(\frac{1}{2} \Omega(r)^2 f(r)^2 - V(f(r)) \right) r^2 dr$$
$$= \Omega_\infty Q_N + 2(E^{(T)} - E^{(P)}). \tag{42}$$

IV. NUMERICAL RESULTS

The system of differential equations (13) and (14) with boundary conditions (15) represents a mixed boundary value problem on the semi-infinite interval $r \in [0, \infty)$, which can be solved only by numerical methods. In this paper, the boundary value problem was solved using the MAPLE package [27]. Since the point $r = 0$ is the regular singular point of the system (13), (14), we apply a difference scheme that does not use the boundary values of the functions. To check the correctness of our numerical solutions, we use Eq. (11) and the Laue condition (32).

The mixed boundary value problem (13)–(15) depends on the five parameters: e, m, g, h, and Ω_∞. To reduce the number of the parameters, we rescale the radial variable and the ansatz functions:

$$r = \frac{\tilde{r}}{m}, \quad f(r) = \frac{m}{\sqrt{g}} \tilde{f}(\tilde{r}), \quad A_0(r) = \frac{m}{\sqrt{g}} \tilde{A}_0(\tilde{r}). \tag{43}$$

After rescaling, the boundary value problem will depend on only the three dimensionless parameters: $\tilde{e} = eg^{-1/2}$, $\tilde{h} = hm^2 g^{-2}$, and $\tilde{\Omega}_\infty = m^{-1}\Omega_\infty$. In particular, the self-interaction potential will depend on only one dimensionless parameter: $V(\tilde{f}) = 2^{-1}\tilde{f}^2 - 8^{-1}\tilde{f}^4 + 24^{-1}\tilde{h}\tilde{f}^6$. Furthermore, the dependences of the Noether charge Q_N, the electric

charge Q, and the energy E on the parameters m and g are factorized as

$$Q_N = g^{-1}\tilde{Q}_N, \quad Q = g^{-1/2}\tilde{Q}, \quad E = mg^{-1}\tilde{E}, \quad (44)$$

where $\tilde{Q}_N$, $\tilde{Q} = \tilde{e}\tilde{Q}_N$, and $\tilde{E}$ are the rescaled versions of the Noether charge, the electric charge, and the energy, respectively. We can therefore without loss of generality set the parameters m and g equal to unity. To avoid spontaneous breaking of the gauge symmetry, the sextic self-interaction coupling constant $\tilde{h}$ must satisfy the inequality $\tilde{h} > 3/16$. In most numerical calculations, we set $\tilde{h} = 0.2$, whereas the remaining parameters $\tilde{e}$ and $\tilde{\Omega}_\infty$ may vary within allowable intervals.

First, let us ascertain the domain in the parameter space in which the basic and radially excited states of the gauged Q-ball can exist. It is shown in Appendix B that the gauged Q-ball solution cannot exist if the gauge coupling constant exceeds some maximum value. Figure 1 shows the dependences of the maximum allowable gauge coupling constant $\tilde{e}_{max}$ on the self-interaction coupling constant $\tilde{h}$ for the basic and the first five radially excited Q-balls. These dependences are presented on the logarithmic scale ranging from the minimum permissible $\tilde{h} = 3/16$ to $\tilde{h} = 50$. We see that for $\tilde{h} \gtrsim 0.5$ all the curves are well described by the formula

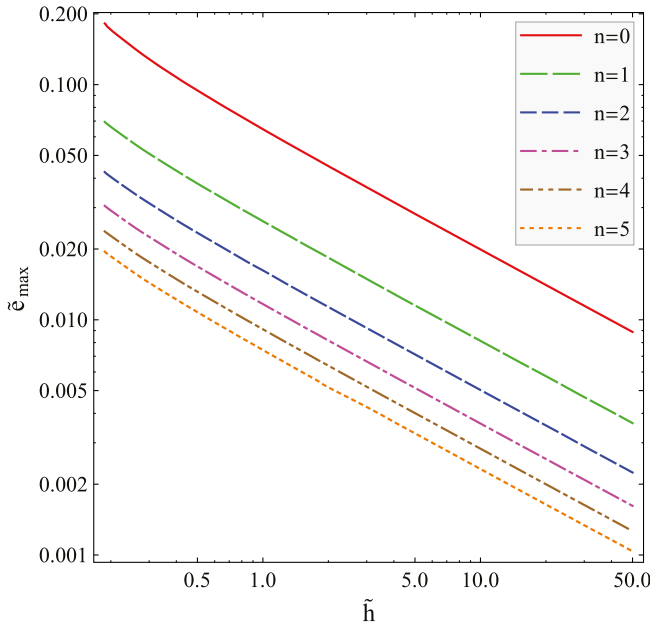$$\tilde{e}_{max} \approx \frac{\epsilon_n}{\sqrt{\tilde{h}}}, \quad (45)$$

FIG. 1.   Dependences of the maximum allowable gauge coupling constant $\tilde{e}_{max}$ on the self-interaction coupling constant $\tilde{h}$ for the basic and first five radially excited Q-ball states.

where ϵ_n are constant coefficients and the label $n = 0, \ldots, 5$ corresponds to the basic and first five radially excited Q-balls.

For large $\tilde{h}$, Eq. (45) can be explained as follows. Let $\tilde{e}$ be equal to zero; then, the electromagnetic field decouples from the complex scalar field, and the ansatz function $\tilde{\Omega}$ becomes the constant phase frequency $\tilde{\omega}$. In this nongauged case, there is an analytical expression for the minimum possible phase frequency: $\tilde{\omega}_{min} = (1 - (3/16)\tilde{h}^{-1})^{1/2} = 1 - (3/32)\tilde{h}^{-1} + O(\tilde{h}^{-2})$. We see that for sufficiently large $\tilde{h}$ the phase frequency $\tilde{\omega}$ lies in the narrow range $(1 - (3/32)\tilde{h}^{-1}, 1)$ with width $\propto \tilde{h}^{-1}$. Next, we turn on the electromagnetic interaction by allowing $\tilde{e}$ to be different from zero, meaning that the phase frequency $\tilde{\omega}$ turns into the monotonically increasing [see Eq. (16a)] function $\tilde{\Omega}(\tilde{r})$. This increase in $\tilde{e}$ leads to an increase in $\tilde{\Omega}_\infty$, which continues until $\tilde{\Omega}_\infty$ reaches the maximum possible value $\tilde{\Omega}_\infty = 1$ at $\tilde{e} = \tilde{e}_{max}$. At the same time, Eqs. (23) and (B1) tell us that for small $\tilde{e}$ the difference $\tilde{\Omega}_\infty - \tilde{\Omega}_0 = \tilde{e}^2\tilde{J}_N + O(\tilde{e}^4)$, where the integral $\tilde{J}_N = \tilde{\omega}\int_0^\infty \tilde{r}\tilde{f}(\tilde{r})^2 d\tilde{r}$ does not depend on $\tilde{e}$. It follows that $\tilde{e}_{max}^2 \propto \tilde{h}^{-1}$ at sufficiently large $\tilde{h}$, resulting in Eq. (45). Note, however, that Eq. (45) becomes valid at $\tilde{h} \gtrsim 0.5$.

From Fig. 1, it follows that in Eq. (45) the coefficients ϵ_n decrease with an increase in n. Thus, the maximum allowable gauge coupling constant $\tilde{e}_{max}$ becomes smaller for the more excited Q-ball solutions. It was found numerically that for $n \gtrsim 3$ the coefficients ϵ_n are well described by the formula

$$\epsilon_n \approx 0.037 n^{-1}. \quad (46)$$

We see that if the point $(\tilde{h}, \tilde{e})$ lies above the solid curve in Fig. 1, then no Q-ball solutions exist with the parameters $\tilde{h}$ and $\tilde{e}$. Moreover, if the gauge coupling constant $\tilde{e}$ exceeds the limiting value 0.182, then there are no Q-ball solutions in model (1). On the other hand, Eqs. (45) and (46) tell us that for a given $\tilde{h}$ the number of radially excited states of the gauged Q-ball is inversely proportional to the gauge coupling constant $\tilde{e}$. Thus, the number of radially excited states increases indefinitely (proportional to $\tilde{e}^{-1}$) as the gauge coupling constant $\tilde{e} \to 0$.

Let a Q-ball solution exist for given values of the parameters $\tilde{e}$ and $\tilde{h}$. In this case, the parameter $\tilde{\Omega}_\infty$ lies in a range from the minimum allowable value $\tilde{\Omega}_\infty^{min}$ to the maximum allowable value of 1. Figure 2 presents the dependences of the minimum allowable value of $\tilde{\Omega}_\infty$ on the gauge coupling constant $\tilde{e}$ for the basic and the first five radially excited Q-ball solutions. In Fig. 2, the curves $\tilde{\Omega}_\infty^{min}(\tilde{e})$ correspond to the self-interaction coupling constant $\tilde{h} = 0.2$; for other values of $\tilde{h}$, the behavior of the curves $\tilde{\Omega}_\infty^{min}(\tilde{e})$ is similar to that in Fig. 2. We see that for a given $\tilde{e}$ the nth radially excited Q-ball solution may exist
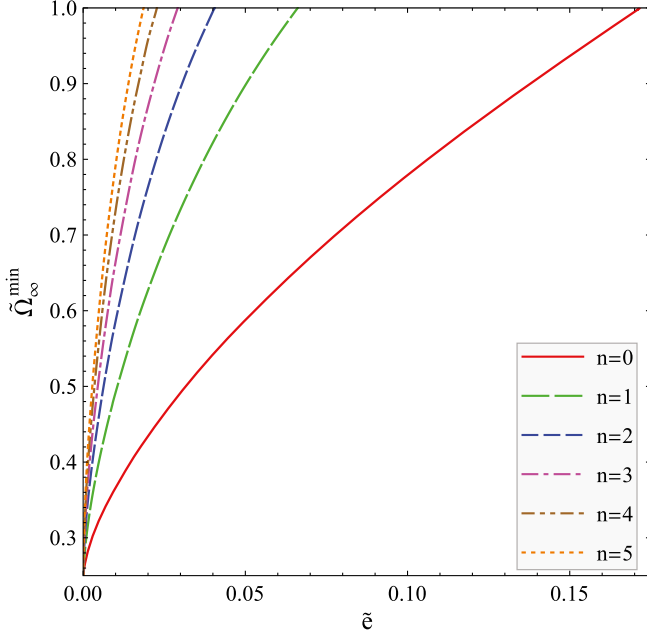
FIG. 2. Dependences of the minimum allowable value of the parameter $\tilde{\Omega}_\infty$ on the gauge coupling constant $\tilde{e}$ for the basic and first five radially excited Q-ball states. The curves correspond to the self-interaction coupling constant $\tilde{h} = 0.2$.

FIG. 3. Curves $\tilde{\Omega}_0(\tilde{\Omega}_\infty)$ for different values of the gauge coupling constant $\tilde{e}$ and the self-interaction coupling constant $\tilde{h} = 0.2$. The curves correspond to the unexcited Q-ball solution. The straight solid line corresponds to the linear dependence $\tilde{\Omega}_0 = \tilde{\Omega}_\infty$.

only if $\tilde{\Omega}_\infty \in [\tilde{\Omega}_\infty^{\min}(\tilde{e}), 1]$, where it is understood that $\tilde{\Omega}_\infty^{\min}(\tilde{e})$ is taken for the corresponding n. When $\tilde{e}$ tends to zero, all the curves in Fig. 2 tend to the minimum possible phase frequency for the nongauged case: $\tilde{\omega}_{\min} = (1 - (3/16)\tilde{h}^{-1})^{1/2}$. As $\tilde{e}$ increases, all the curves monotonically increase until the maximum possible value $\tilde{\Omega}_\infty = 1$ is reached. In Fig. 2, the intersection points of the curves and the line $\tilde{\Omega}_\infty = 1$ represent the maximum allowable gauge coupling constants corresponding to the self-interaction constant $\tilde{h} = 0.2$ in Fig. 1. In particular, it follows from Fig. 2 that in accordance with Fig. 1 the maximum allowable gauge coupling constant $\tilde{e}_{\max}$ decreases with an increase in the radial excitation of the Q-ball solution.

It is shown in Appendix B that the restriction $\Delta\Omega < m$ on the difference $\Delta\Omega = \Omega_\infty - \Omega_0$ prevents the existence of gauged Q-balls with an arbitrarily large electric charge or gauge coupling constant. However, the parameters Ω_0 and Ω_∞ are not independent, since they are both determined by the solution to the mixed boundary value problem (13)–(15). In this connection, it would be interesting to study the dependence $\tilde{\Omega}_0(\tilde{\Omega}_\infty)$ for different values of the gauge coupling constant as well as for different radially excited Q-ball solutions. Figure 3 shows the dependences $\tilde{\Omega}_0(\tilde{\Omega}_\infty)$ for the unexcited Q-ball solution corresponding to different values of the gauge coupling constant $\tilde{e}$. We see that for nonzero $\tilde{e}$ all the curves $\tilde{\Omega}_0(\tilde{\Omega}_\infty)$ intersect the line $\tilde{\Omega}_\infty = 1$ at two points, and thus each of these curves has a turning point at $\tilde{\Omega}_\infty = \tilde{\Omega}_\infty^{\min}$, where the derivative
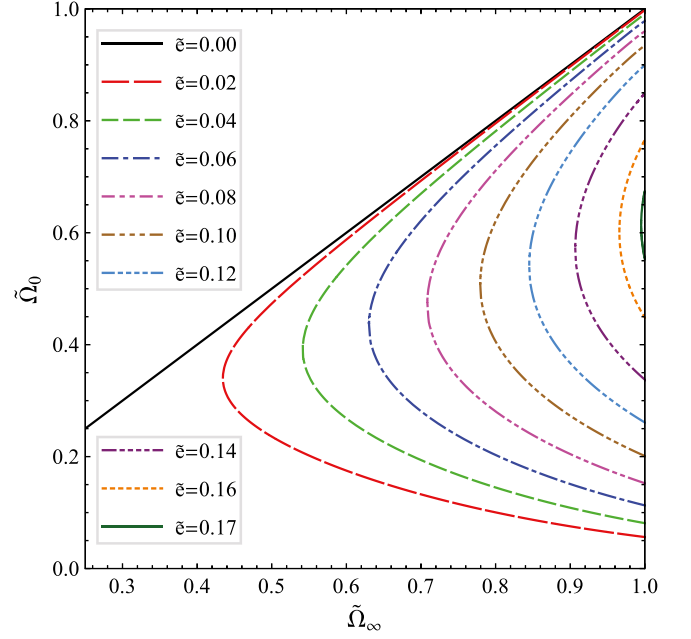
$d\tilde{\Omega}_0/d\tilde{\Omega}_\infty$ becomes infinite. In Fig. 3, the dependence of $\tilde{\Omega}_\infty^{\min}$ on $\tilde{e}$ is described by the solid curve in Fig. 2. In particular, it follows from Fig. 2 that $1 - \tilde{\Omega}_\infty^{\min} \propto \tilde{e}_{\max} - \tilde{e}$ in the vicinity of the maximum allowable gauge coupling constant $\tilde{e}_{\max}$. This means that the allowable interval of $\tilde{\Omega}_\infty$ shrinks to a point as $\tilde{e} \to \tilde{e}_{\max}$ and thus the gauged Q-ball cannot exist if $\tilde{e} \geq \tilde{e}_{\max}$. From Fig. 3, it follows that the parameter $\tilde{\Omega}_\infty$ does not uniquely define the gauged Q-ball solution, since there exist two different Q-ball solutions for each $\tilde{\Omega}_\infty \in (\tilde{\Omega}_\infty^{\min}, 1]$. At the same time, Fig. 3 tells us that the gauged Q-ball solution is uniquely defined by the parameter $\tilde{\Omega}_0$. The curves shown in Fig. 3 correspond to the basic ($n = 0$) Q-ball solution; for the radially excited Q-ball solutions ($n \geq 1$), the behavior of the curves $\tilde{\Omega}_0(\tilde{\Omega}_\infty)$ is similar to that in Fig. 3.

Now, we discuss the behavior of gauged Q-balls as the gauge coupling constant $\tilde{e}$ tends to zero. From Fig. 3, it follows that turning points divide the curves $\tilde{\Omega}_0(\tilde{\Omega}_\infty)$ into upper and lower branches. In the limit $\tilde{e} \to 0$, the $\tilde{\Omega}_\infty$ coordinate of the turning point tends to the nongauged value $\tilde{\omega}_{\min} = (1 - (3/16)\tilde{h}^{-1})^{1/2}$, and thus gauged Q-ball solutions that lie on the upper branch tend to the corresponding nongauged ones on the straight line $\tilde{\Omega}_0 = \tilde{\Omega}_\infty$. In contrast, gauged Q-ball solutions that lie on the lower branch do not tend to nongauged ones as $\tilde{e} \to 0$. It can be said that as $\tilde{e} \to 0$ the gauge field decouples from Q-ball solutions lying on the upper branch of the curve $\tilde{\Omega}_0(\tilde{\Omega}_\infty)$
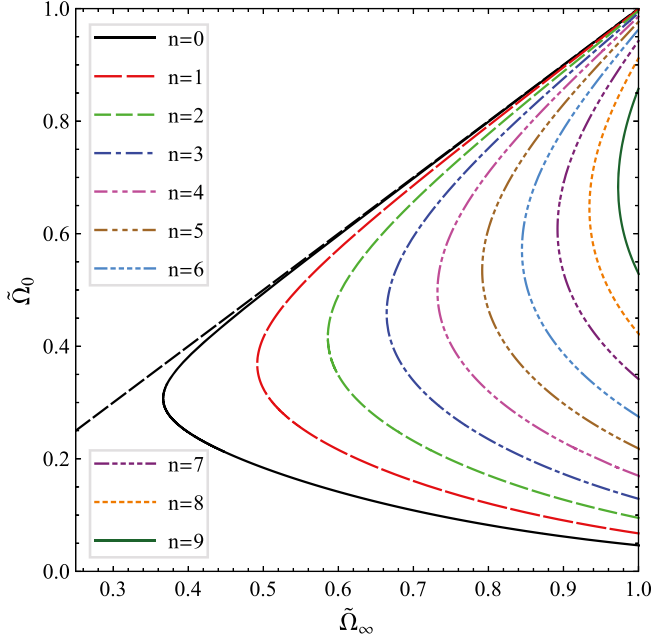
FIG. 4. Curves $\tilde{\Omega}_0(\tilde{\Omega}_\infty)$ for the unexcited and first nine radially excited Q-ball solutions. The curves correspond to the parameters $\tilde{e} = 0.01$ and $\tilde{h} = 0.2$. The straight dashed line corresponds to the linear dependence $\tilde{\Omega}_0 = \tilde{\Omega}_\infty$.

but does not decouple from those lying on the lower branch. Indeed, in this limit, the difference $\Delta\tilde{\Omega} = \tilde{\Omega}_\infty - \tilde{\Omega}_0 \to 0$ for Q-ball solutions on the upper branch, whereas $\Delta\tilde{\Omega} \to \tilde{\Omega}_\infty - \tilde{\omega}_{\min}$ for Q-ball solutions on the lower branch. It follows that for Q-ball solutions that lie on the lower branch the integral $\tilde{J} = \int_0^\infty \tilde{r}\tilde{j}_0(\tilde{r})d\tilde{r}$ on the right-hand side of Eq. (B1) increases indefinitely as $\tilde{e} \to 0$. Hence, the electric charge $\tilde{Q} = 4\pi\int_0^\infty \tilde{r}^2\tilde{j}_0(\tilde{r})d\tilde{r}$, the Noether charge $\tilde{Q}_N = \tilde{e}^{-1}\tilde{Q}$, and the energy $\tilde{E}$ of these Q-ball solutions also increase indefinitely in this limit.

Now, let us consider the curves $\tilde{\Omega}_0(\tilde{\Omega}_\infty)$ for the radially excited Q-ball solutions. Figure 4 shows these curves for the unexcited ($n = 0$) and the first nine radially excited ($n = 1, \ldots, 9$) gauged Q-balls corresponding to the parameters $\tilde{e} = 0.01$ and $\tilde{h} = 0.2$. We see that in Fig. 4 the behavior of the curves is similar to that in Fig. 3. Indeed, all the curves in Fig. 4 intersect the limiting line $\tilde{\Omega}_\infty = 1$ at two points and have a turning point with the infinite derivative $d\tilde{\Omega}_0/d\tilde{\Omega}_\infty$. This similarity can be explained as follows. Equations (45) and (46) tell us that for the nth radially excited Q-ball solution the maximum allowable gauge coupling constant $\tilde{e}_{\max} \propto n^{-1}$. It follows that for the curves in Fig. 4 the difference $\tilde{e}_{\max} - \tilde{e}$ decreases with an increase in n due to the decrease in $\tilde{e}_{\max}$. A similar situation is observed in Fig. 3, where the difference $\tilde{e}_{\max} - \tilde{e}$ decreases due to the increase in $\tilde{e}$ at fixed $\tilde{e}_{\max}$. In both cases, the decrease in the difference $\tilde{e}_{\max} - \tilde{e}$ leads to a decrease in the allowable interval of $\tilde{\Omega}_\infty$. The decrease in

the interval of $\tilde{\Omega}_\infty$ results in the existence of the maximum radially excited Q-ball solution for a given $\tilde{e}$ (the solution with $n = 9$ in Fig. 4). Note that for a given $\tilde{e}$ the existence of the maximum radially excited gauged Q-ball is in accordance with Eqs. (45) and (46).

Next, we turn to a study of the dependence of the energy $\tilde{E}$ on the parameter $\tilde{\Omega}_\infty$ for the gauged Q-ball solutions. The dependence $\tilde{Q}_N(\tilde{\Omega}_\infty)$ is similar to $\tilde{E}(\tilde{\Omega}_\infty)$ and is therefore not shown. In Fig. 5, we can see the curves $\tilde{E}(\tilde{\Omega}_\infty)$ for the different values of the gauge coupling constant $\tilde{e}$. These curves correspond to the unexcited Q-ball solution. The curves $\tilde{E}(\tilde{\Omega}_\infty)$ corresponding to the radially excited Q-ball solutions are similar to those in Fig. 5 and are not shown. First, we see that the behavior of the curve $\tilde{E}(\tilde{\omega})$ for the nongauged case $\tilde{e} = 0$ (for which the parameter $\tilde{\Omega}_\infty$ is equal to the phase frequency $\tilde{\omega}$) is drastically different from that for the gauged case $\tilde{e} \neq 0$. Indeed, the energy of the nongauged Q-ball with the self-interaction potential (5) tends to infinity both in the thin-wall regime $\tilde{\omega} \to \tilde{\omega}_{\min} = (1 - (3/16)\tilde{h}^{-1})^{1/2}$, where $\tilde{E} \propto (\tilde{\omega}^2 - \tilde{\omega}_{\min}^2)^{-3}$, and in the thick-wall regime $\tilde{\omega} \to 1$, where $\tilde{E} \propto (1 - \tilde{\omega}^2)^{-1/2}$. At the same time, the energy of any gauged Q-ball remains finite for all $\tilde{\Omega}_\infty \in [\tilde{\Omega}_\infty^{\min}, 1]$, where the minimum possible value $\tilde{\Omega}_\infty^{\min}$ depends on $\tilde{e}$ in accordance with Fig. 2. We see again that for a given $\tilde{\Omega}_\infty$ there exist the two gauged Q-ball solutions whose energies can differ by several orders of magnitude. In particular, the curves $\tilde{E}(\tilde{\Omega}_\infty)$ intersect the limiting line $\tilde{\Omega}_\infty = 1$ at two points. It was found numerically that for the Q-ball solutions corresponding to the upper intersection points
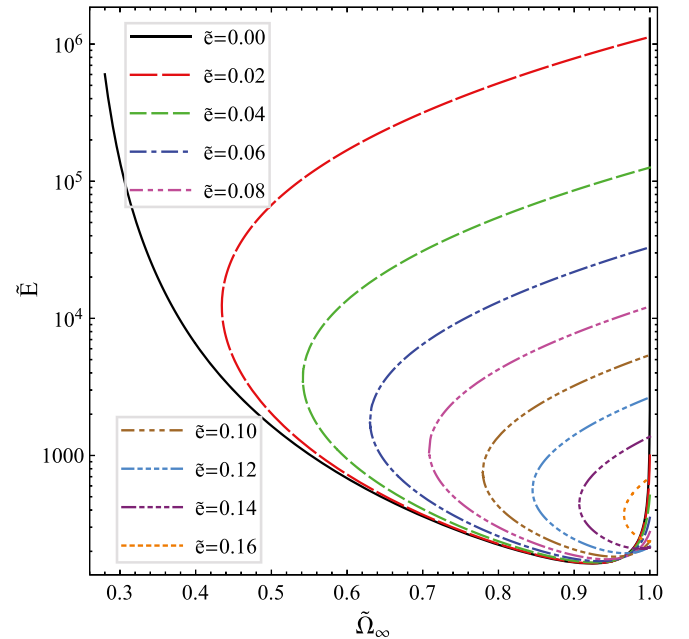

FIG. 5. Curves $\tilde{E}(\tilde{\Omega}_\infty)$ for different values of $\tilde{e}$ and $\tilde{h} = 0.2$. The curves correspond to the unexcited Q-ball solution.

the energy, Noether charge, and electric charge increase indefinitely as $\tilde{e} \to 0$,

$$\tilde{E} \sim \bar{\varepsilon}\tilde{e}^{-3}, \qquad \tilde{Q}_N \sim \bar{q}_N\tilde{e}^{-3}, \qquad \tilde{Q} \sim \bar{q}_N\tilde{e}^{-2}, \quad (47)$$

where $\bar{\varepsilon}$ and $\bar{q}_N$ are dimensionless functions of the self-interaction coupling constant $\tilde{h}$. It can be said that for sufficiently small $\tilde{e}$ the gauged Q-ball that corresponds to the upper intersection point passes into the quasi-thin-wall regime described in Ref. [14].

The $\tilde{e}$ dependences in Eq. (47) can be explained qualitatively as follows. The basic property of the thin-wall regime is that the ansatz functions $\tilde{f}(\tilde{r})$ and $\tilde{\Omega}(\tilde{r})$ are approximately constant for $\tilde{r} \in [0, \tilde{R})$, where $\tilde{R}$ can be arbitrarily large in the true thin-wall regime (nongauged case) and large but finite in the quasi-thin-wall regime (gauged case). Equation (13) tells us that $\tilde{f}(\tilde{r})$ can be almost constant on the interval $[0, \tilde{R})$ only if $(\tilde{\Omega}^2 - 1)\tilde{f} + \tilde{f}^3/2 - \tilde{h}\tilde{f}^5/4 \approx 0$ there. It follows that in the quasi-thin-wall regime

$$\tilde{f}_0 \approx \tilde{h}^{-\frac{1}{2}}[1 + (1 - 4\tilde{h}(1 - \tilde{\Omega}_0^2))^{\frac{1}{2}}]^{\frac{1}{2}}, \qquad (48)$$

where $\tilde{\Omega}_0$ and $\tilde{f}_0$ are the values of the corresponding ansatz functions at $\tilde{r} = 0$. However, the term $\tilde{e}^2\tilde{\Omega}\tilde{f}^2$ in Eq. (14) does not allow the ansatz function $\tilde{\Omega}(\tilde{r})$ to be approximately constant on the interval $[0, \tilde{R})$ with an arbitrary large $\tilde{R}$; hence, there is no true thin-wall regime in model (1), and as a consequence, there is no gauged Q-ball possessing an arbitrarily large Noether (and, consequently, electric) charge. From Eq. (17b), it follows that $\tilde{\Omega}(\tilde{r}) \approx \tilde{\Omega}_0 + \tilde{e}^2\tilde{f}_0^2\tilde{\Omega}_0\tilde{r}^2/6$. We see that $\tilde{\Omega}(\tilde{r})$ will be approximately constant on the interval $[0, \tilde{R})$ until $\tilde{e}\tilde{f}_0\tilde{R} \ll 1$. It follows that

$$\tilde{R} \approx \varrho\tilde{f}_0^{-1}\tilde{e}^{-1}, \qquad (49)$$

where the constant $\varrho \ll 1$. Hence, the volume of the ball in which the ansatz functions $\tilde{\Omega}_0$ and $\tilde{f}_0$ are approximately constant is proportional to $\tilde{e}^{-3}$. Next, Eqs. (23) and (24) tell us that the Noether charge and energy densities are also approximately constant inside the ball of radius $\tilde{R} \propto \tilde{e}^{-1}$, and this gives rise to Eq. (47).

In the nongauged case, the Q-ball passes into the thick-wall regime as $\tilde{\omega} \to 1$. In this regime, the amplitude $\tilde{f}$ of the complex scalar field tends to zero as $(1 - \tilde{\omega}^2)^{1/2}$, and thus the nongauged Q-ball solution spreads over the space. It was shown in Ref. [8] that for the potential (5), the energy and Noether charge of the thick-wall nongauged Q-ball diverge as $(1 - \tilde{\omega}^2)^{-1/2}$. Conversely, it follows from Fig. 5 that for fixed $\tilde{e}$ the energy of the Q-ball solution corresponding to the lower intersection point remains finite at $\tilde{\omega} = 1$. The amplitude $\tilde{f}$ also remains finite, and thus there

is no thick-wall regime when the gauge coupling constant $\tilde{e}$ is fixed [24]. However, it was found numerically that at the lower intersection point the energy and Noether charge of the gauged Q-ball diverge as $\tilde{e} \to 0$,

$$\tilde{E} \approx \tilde{Q}_N \sim \bar{\bar{q}}_N\tilde{e}^{-1}, \qquad (50)$$

whereas the electric charge $\tilde{Q} = \tilde{e}\tilde{Q}_N$ remains finite. This behavior can be explained as follows. In the unitary gauge, the parameter $\tilde{\Omega}_\infty$ plays the same role as the phase frequency $\tilde{\omega}$ in the nongauged case. From Fig. 3, it follows that at $\tilde{\Omega}_\infty = 1$ the difference $\tilde{\mu}^2 = 1 - \tilde{\Omega}_0^2$ tends to zero as $\tilde{e} \to 0$. Next, it is shown in Appendix B that for small values of the parameter $\tilde{\mu}$ the Noether charge $\tilde{Q}_N \propto \tilde{\mu}^{-1}$. However, the integral $\tilde{J} = \tilde{e}\int_0^\infty \tilde{r}\tilde{j}_0(\tilde{r})d\tilde{r}$ on the right-hand side of Eq. (B1) is proportional to $\tilde{e}^2$, whereas the left-hand side of Eq. (B1) is proportional to $\tilde{\mu}^2/2$. It follows that for small $\tilde{e}$ the parameter $\tilde{\mu} \propto \tilde{e}$ and thus $\tilde{E} \approx \tilde{Q}_N \propto \tilde{\mu}^{-1} \propto \tilde{e}^{-1}$, in accordance with the numerical results.

In Fig. 5, all the curves (except for the one corresponding to the nongauged case $\tilde{e} = 0$) have turning points at which the derivative $d\tilde{E}/d\tilde{\Omega}_\infty$ becomes infinite. Equation (11) tells us that $d\tilde{Q}_N/d\tilde{\Omega}_\infty$ is also infinite at the turning points, and thus the derivative $d\tilde{\Omega}_\infty/d\tilde{Q}_N$ vanishes at these points. This means that the second derivative $d^2\tilde{E}/d\tilde{Q}_N^2 = d\tilde{\Omega}_\infty/d\tilde{Q}_N$ also vanishes at these turning points, and thus the turning points on the curves $\tilde{E}(\tilde{\Omega}_\infty)$ correspond to the inflection points of the curves $\tilde{E}(\tilde{Q}_N)$. The curve $\tilde{E}(\tilde{Q}_N)$ therefore has one inflection point in the gauged case, whereas it has no inflection points in the nongauged case. These facts can be explained qualitatively as follows. The derivative $d\tilde{E}/d\tilde{\Omega}_\infty$ determines the profitability of the absorption of the scalar ϕ-boson into the Q-ball from the viewpoint of the energy balance. Indeed, the quantity $m(1 - d\tilde{E}/d\tilde{Q}_N)$ is the energy needed to extract one scalar ϕ-boson from the Q-ball with Noether charge Q_N and to transport the extracted ϕ-boson to infinity. From Eq. (11), it follows that the derivative $d\tilde{E}/d\tilde{Q}_N$ decreases monotonically with a decrease in $\tilde{\Omega}_\infty$. It than follows from Fig. 5 that for the nongauged Q-ball solutions lying on the left (thin-wall) part of the curve $\tilde{E}(\tilde{\Omega}_\infty)$ the derivative $d\tilde{E}/d\tilde{Q}_N$ decreases monotonically with an increase in $\tilde{Q}_N$ and thus the difference $(m + E(Q_N - 1)) - E(Q_N) \approx m(1 - d\tilde{E}/d\tilde{Q}_N)$ increases monotonically with an increase in $\tilde{Q}_N$. We conclude that in the nongauged case $\tilde{e} = 0$ the absorption of the ϕ-boson becomes more energetically profitable with an increase in the Q-ball's Noether charge toward the thin-wall regime. The situation changes drastically for gauged Q-balls. In this case, the role of the electrostatic Coulomb repulsion increases with an increase in the Noether (and consequently the electric) charge. The long-range Coulomb repulsion means that the absorption of the ϕ-boson into a gauged Q-ball with Noether charge Q_N is less profitable

energetically in comparison with the absorption of the ϕ-boson into a nongauged Q-ball with the same Q_N. Hence, for the same Q_N, the difference $[m + E(Q_N - 1)) - E(Q_N) \approx m(1 - d\tilde{E}/d\tilde{Q}_N]$ is smaller for the gauged Q-ball than for the nongauged one, and thus $d\tilde{E}_g/d\tilde{Q}_N > d\tilde{E}_{ng}/d\tilde{Q}_N$, where $\tilde{E}_g$ and $\tilde{E}_{ng}$ are the energies of the gauged and nongauged Q-balls, respectively. The difference $d\tilde{E}_g/d\tilde{Q}_N - d\tilde{E}_{ng}/d\tilde{Q}_N$ increases with an increase in $\tilde{Q}_N$, leading to the inflection points on the curves $\tilde{E}(\tilde{Q}_N)$ in the gauged case (see Fig. 6) and, as a consequence, to the turning points on the curves $\tilde{E}(\tilde{\Omega}_\infty)$ in Fig. 5. In Appendix C, the existence of the inflection point on the curve $\tilde{E}(\tilde{Q}_N)$ is explained analytically within a certain approximation.

Figure 6 presents the curves $\tilde{E}(\tilde{Q}_N)$ for the first few values of the gauge coupling constant $\tilde{e}$ and the self-interaction coupling constant $\tilde{h} = 0.2$. For $\tilde{e} = 0.02$ and $\tilde{e} = 0.04$, two characteristic points of the curve $\tilde{E}(\tilde{Q}_N)$ are shown: the inflection point, where $d^2\tilde{E}/d\tilde{Q}_N^2 = 0$, and the point of contact, where $d\tilde{E}/d\tilde{Q}_N = \tilde{E}/\tilde{Q}_N$. The inflection points lie to the left of the corresponding points of contact. For $\tilde{e} = 0.06$, the terminal point corresponding to the maximum allowable Noether charge and energy is shown, whereas the inflection point and the point of contact are not shown due to their indistinguishability. At the terminal point, the derivative $d\tilde{E}/d\tilde{Q}_N = 1$, in accordance with
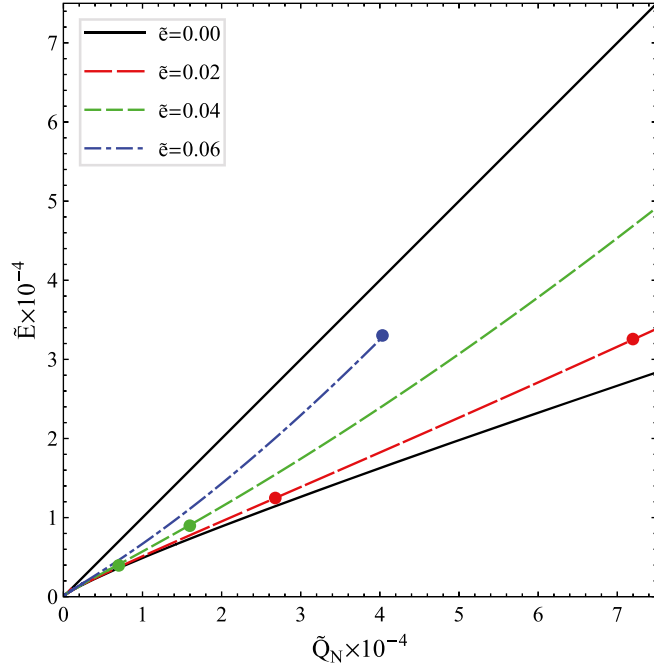
Eq. (11) and Fig. 5. From Fig. 6, it follows that the Q-ball's energy increases rapidly both with an increase in $\tilde{e}$ for fixed $\tilde{Q}_N$ and with an increase in $\tilde{Q}_N$ for fixed $\tilde{e}$.

Figure 7 presents the dependence of the ratio $\tilde{E}/\tilde{Q}_N$ on the Noether charge $\tilde{Q}_N$ for different values of the gauge coupling constant $\tilde{e}$. The curves in Fig. 7 correspond to the unexcited Q-ball solutions. The corresponding curves for the radially excited Q-ball solutions are similar to those in Fig. 7, and thus are not shown. As in the previous figures, the curve for the nongauged Q-ball differs sharply from those for the gauged Q-balls. First, we see that in accordance with Fig. 5 the energy and Noether charge of the nongauged Q-ball increase indefinitely, both in the thin-wall ($\tilde{E}/\tilde{Q}_N \to \tilde{\omega}_{min}$) and in the thick-wall ($\tilde{E}/\tilde{Q}_N \to 1$) regimes, whereas there are upper bounds on the energy and Noether charge of the gauged Q-balls. Next, in Fig. 7, all the curves (except those that correspond to $\tilde{e} = 0.14$ and $\tilde{e} = 0.16$) have cuspidal points; these points correspond to the minima of the curves $\tilde{E}(\tilde{\Omega}_\infty)$ in Fig. 5. Note that, due to Eq. (11), the position of the minimum in the curve $\tilde{E}(\tilde{\Omega}_\infty)$ coincides with that in the corresponding curve $\tilde{Q}_N(\tilde{\Omega}_\infty)$, giving rise to the cusps in Fig. 7. In Fig. 5, the curves $\tilde{E}(\tilde{\Omega}_\infty)$ with $\tilde{e} = 0.14$ and $\tilde{e} = 0.16$ have no minima, resulting in the absence of cusps for the corresponding curves in Fig. 7. We see that for all of the curves the ratio $\tilde{E}/\tilde{Q}_N$ reaches a maximum value at the point (cuspidal or otherwise) with the minimum possible Noether charge $\tilde{Q}_N$.
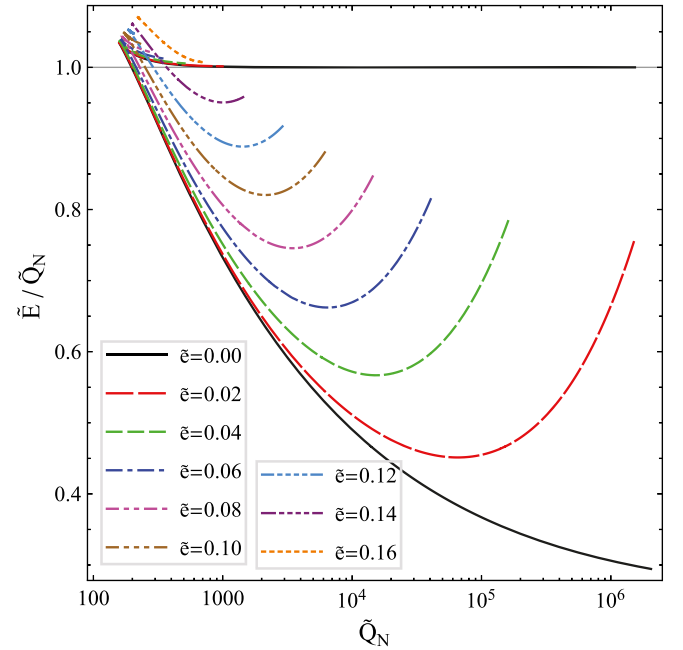

FIG. 6. Curves $\tilde{E}(\tilde{Q}_N)$ for the first few values of $\tilde{e}$ and $\tilde{h} = 0.2$. The inflection point (on the left) and the point of contact (on the right) are shown both for $\tilde{e} = 0.02$ and $\tilde{e} = 0.04$. The terminal point is shown for $\tilde{e} = 0.06$. The curves correspond to the unexcited Q-ball solution.

FIG. 7. Dependence of the ratio $\tilde{E}/\tilde{Q}_N$ on the Noether charge $\tilde{Q}_N$ for different values of $\tilde{e}$ and $\tilde{h} = 0.2$. The curves correspond to the unexcited Q-ball solution.

In Fig. 7, all the curves corresponding to gauged Q-balls (except the one corresponding to $\tilde{e} = 0.16$) have global minima, whereas the curve that corresponds to the non-gauged Q-ball has no minimum. It can easily be shown that at the minimum point $d\tilde{E}/d\tilde{Q}_N = \tilde{E}/\tilde{Q}_N$ and $d^2(\tilde{E}/\tilde{Q}_N)/d\tilde{Q}_N^2 = (d^2\tilde{E}/d\tilde{Q}_N^2)/\tilde{Q}_N$. From Fig. 7, it follows that the derivative $d^2(\tilde{E}/\tilde{Q}_N)/d\tilde{Q}_N^2$ is positive at the minimum points, and thus the derivative $d^2\tilde{E}/d\tilde{Q}_N^2$ is also positive there. Hence, the curve $\tilde{E}(\tilde{Q}_N)$ has a convex downward shape at the minimum point of $\tilde{E}(\tilde{Q}_N)/\tilde{Q}_N$; this is consistent with the existence of inflection points for the curves with nonzero $\tilde{e}$ in Fig. 6. It also follows from Fig. 6 that the curve for zero $\tilde{e}$ has no inflection point, due to the absence of a minimum point for the curve for zero $\tilde{e}$ in Fig. 7.

At the minimum point of the curve $\tilde{E}(\tilde{Q}_N)/\tilde{Q}_N$, the derivative $d\tilde{E}/d\tilde{Q}_N = \tilde{E}/\tilde{Q}_N$, and this point therefore corresponds to the point of contact between the curve $\tilde{E}(\tilde{Q}_N)$ and the straight line passing through the origin of coordinates. From Fig. 6, it follows that the inflection point lies to the left of the point of contact. Hence, it is possible that the curve $\tilde{E}(\tilde{Q}_N)$ terminates after the inflection point but has no point of contact with the straight line passing through the origin of coordinates. In Fig. 7, this situation is seen for the curve with $\tilde{e} = 0.16$, which has no minimum.

In Fig. 7, the cuspidal points divide the curves into upper and lower branches, and the curves without cuspidal points (corresponding to $\tilde{e} = 0.14$ and $\tilde{e} = 0.16$) have only one branch. We see that for nonzero $\tilde{e}$ both the lower branches of the double-branch curves and the single-branch curves terminate at the rightmost points. These points correspond to the Q-ball solutions with maximum energy and Noether charge for a given $\tilde{e}$. From Eq. (11) and Figs. 3 and 5, it follows that for these Q-ball solutions the derivative $d\tilde{E}/d\tilde{Q}_N = 1$ (and consequently $dE/dQ_N = m$). Similarly, the derivative $d\tilde{E}/d\tilde{Q}_N$ is also equal to unity at the rightmost points of the upper branches of the curves and at the leftmost points of the single-branch curves. We see that the gauged Q-balls cease to exist at the points where the derivative dE/dQ_N is equal to the mass of the scalar ϕ-boson [14]. Of course, the reason for this lies in Eqs. (11) and (20). The former relation tells us that the parameter $\Omega_\infty = m$ at the points where the derivative $dE/dQ_N = m$, while the latter means that the amplitude of the complex scalar field becomes oscillating when $\Omega_\infty > m$. This implies that the Noether charge and energy become infinite as $\Omega_\infty > m$, and thus the Q-ball solution does not exist in this case.

It follows from Fig. 7 that at fixed $\tilde{Q}_N$ the ratio $\tilde{E}/\tilde{Q}_N$ increases with an increase in $\tilde{e}$ for Q-ball solutions on both upper and lower branches of the curves $\tilde{E}(\tilde{Q}_N)/\tilde{Q}_N$. This is apparently related to the increase in the role of long-range Coulomb repulsion. We also see that the ratio $\tilde{E}/\tilde{Q}_N$ is less than unity for Q-balls with the maximum possible energy

and Noether charge (except for $\tilde{e} = 0.16$). It was found numerically that for these Q-balls the ratio $\tilde{E}/\tilde{Q}_N$ tends to a constant as $\tilde{e} \to 0$, and the constant is approximately equal to 0.73. At the same time, for the nongauged Q-ball, the ratio $\tilde{E}/\tilde{Q}_N$ tends to $\tilde{\omega}_{min} = (1 - (3/16)\tilde{h}^{-1})^{1/2} = 0.25$ when $\tilde{E}$ and $\tilde{Q}_N$ tend to infinity in the thin-wall regime. It follows that for gauged Q-balls the ratio $\tilde{E}/\tilde{Q}_N$ does not tend to the nongauged value of 0.25 as $\tilde{e} \to 0$. Hence, in the limit of vanishing $\tilde{e}$, the gauge field does not decouple from the Q-ball with the maximum possible energy and Noether charge in consistency with the conclusion obtained in analysis of Fig. 3. Note that for the gauged Q-ball with an arbitrarily small $\tilde{e}$ and maximum possible $\tilde{Q}_N$ the ratio $\tilde{E}/\tilde{Q}_N$ is distinctly greater than that for the nongauged Q-ball in the thin-wall regime. Of course, this difference is due to the contribution of the electrostatic energy (35a) to the total energy of gauged Q-ball.

Figure 8 shows the curves $\tilde{E}(\tilde{\Omega}_\infty)$ for the unexcited and first nine radially excited Q-ball solutions. As in Fig. 7, all the curves in Fig. 8 intersect the limiting line $\tilde{\Omega}_\infty = 1$ at two points and possess turning points. We see that in the same way as in Fig. 2 the $\tilde{\Omega}_\infty$ coordinate of the turning point increases monotonically toward the limiting value $\tilde{\Omega}_\infty = 1$ with an increase in n. We also see that the maximum possible energy of a radially excited gauged Q-ball decreases monotonically with an increase in n. Note that such behavior is similar to that shown in Fig. 5, where the maximum possible energy of the unexcited gauged
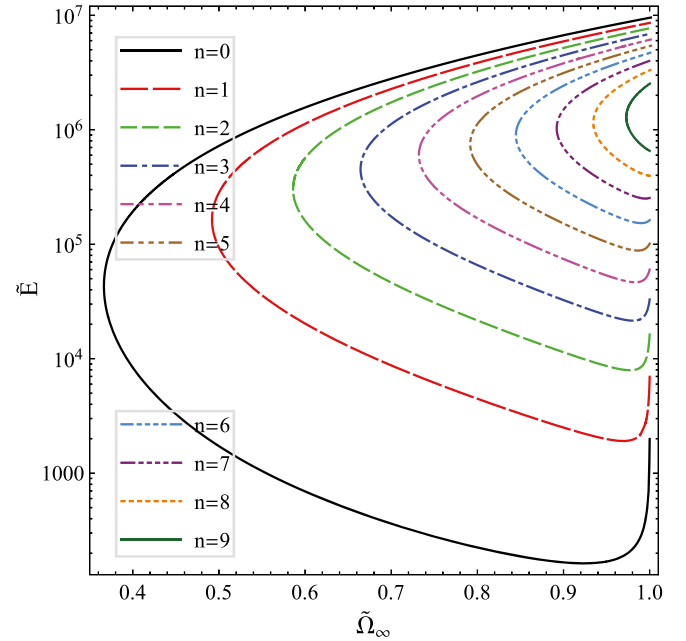

FIG. 8. Curves $\tilde{E}(\tilde{\Omega}_\infty)$ for the unexcited and first nine radially excited Q-ball solutions. The curves correspond to parameters $\tilde{e} = 0.01$ and $\tilde{h} = 0.2$.

FIG. 9. Dependence of the ratio $\tilde{E}/\tilde{Q}_N$ on the Noether charge $\tilde{Q}_N$ for the unexcited and first nine radially excited Q-ball solutions. The curves correspond to parameters $\tilde{e} = 0.01$ and $\tilde{h} = 0.2$.
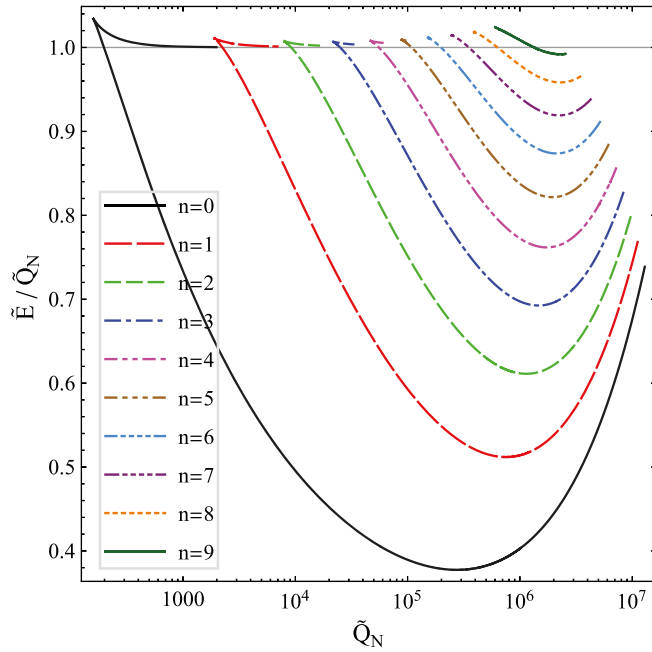
Q-ball decreases monotonically with an increase in the gauge coupling constant $\tilde{e}$.

Next, we turn to Fig. 9, in which the dependence of the ratio $\tilde{E}/\tilde{Q}_N$ on the Noether charge $\tilde{Q}_N$ is shown for the unexcited and first nine radially excited Q-ball solutions. We see that the individual behavior of the curves in Fig. 9 is similar to that in Fig. 7. However, the relative positions of the curves in Fig. 9 are different from those in Fig. 10, since the cusps (or the leftmost points for $n = 8, 9$) in Fig. 9 are separated by larger intervals of $\tilde{Q}_N$ than those in Fig. 7. All the curves $\tilde{E}(\tilde{Q}_N)/\tilde{Q}_N$ in Fig. 9 (except the one corresponding to $n = 9$) have minimum points. With the existence of the turning points in Fig. 8, this implies that the all corresponding curves $\tilde{E}(\tilde{Q}_N)$ have inflection points at which $d^2\tilde{E}/d\tilde{Q}_N^2 = 0$ and (except for $n = 9$) points of contact at which $d\tilde{E}/d\tilde{Q}_N = \tilde{E}/\tilde{Q}_N$. All the curves in Fig. 9 possess two terminal points corresponding to the two points of intersection with the line $\tilde{\Omega}_\infty = 1$ in Fig. 8. This implies that at the terminal points the derivative $d\tilde{E}/d\tilde{Q}_N = 1$. Note that in Fig. 9, the ratio $\tilde{E}/\tilde{Q}_N$ is less than unity at all of the terminal points at the right; for a given n, the right terminal point corresponds to the Q-ball solution with the maximum allowable energy and Noether charge. Finally, it follows from Fig. 9 that for fixed $\tilde{Q}_N$ the energy of the Q-ball solution increases with an increase in n.

Let us discuss the stability of radially excited gauged Q-balls. Figure 9 tells us that for the nth radially excited gauged Q-ball there are at least the n gauged Q-balls

having the same Noether charge but lower energy. It follows that all radially excited gauged Q-balls are unstable with respect to the transition into less excited ones. The energy released in this transition is carried away by the electromagnetic radiation and the scalar ϕ-bosons. Moreover, from Fig. 9, it follows that for all n there are gauged Q-ball solutions (those for which the ratio $\tilde{E}/\tilde{Q}_N > 1$) that are unstable against decay into the massive scalar ϕ-bosons. Thus, all the radially excited gauged Q-balls are unstable. The instability, however, can be either classical (the presence of one or more unstable modes in the functional neighborhood of gauged Q-ball) or quantum mechanical (the possibility of quantum tunneling). Note that the issue of classical stability of gauged Q-balls is rather complicated. Indeed, unlike the nongauged case, there is no criterion of classical stability for gauged Q-balls [28]. Note, however, that in Fig. 9 there are cusps on the curves corresponding to $n = 0, \ldots, 6$. It was shown in Refs. [29,30] that the appearance of a cusp indicates the onset of a new mode of instability. Hence, the curves with cusp have areas of classical instability. At the same time, the presence of cusp may mean the addition of a new unstable mode to already existing ones. In this case, all the radially excited gauged Q-balls would be classically instable as in the model [4].

The boundary conditions (15) and Eq. (28) tell us that the pressure p_0 at the center of the Q-ball solution can be written as

$$p_0 \equiv m^4 g^{-1} \tilde{p}_0 = m^4 g^{-1} \left[\frac{1}{2} \tilde{\Omega}_0^2 \tilde{f}_0^2 - V(\tilde{f}_0) \right], \quad (51)$$

where $\tilde{\Omega}_0 = \tilde{\Omega}(0)$ and $\tilde{f}_0 = \tilde{f}(0)$. In Eq. (51), the expression in square brackets is the dimensionless version of the effective potential (B5): $\tilde{U}_{\text{eff}}(\tilde{f}) = \tilde{\Omega}^2 \tilde{f}^2/2 - V(\tilde{f})$. In the nongauged case, the ansatz function $\tilde{\Omega}(\tilde{r})$ becomes the constant phase frequency $\tilde{\omega}$. It is well known that in this case the value of the effective potential is always positive at the center of the Q-ball solution; hence, the pressure at the center of the nongauged Q-ball solution is also always positive. The situation is different in the gauged case, however, as the effective potential $\tilde{U}_{\text{eff}}(\tilde{f})$ may be negative at $\tilde{r} = 0$, resulting in negative pressure at the center of the gauged Q-ball [24]. Figures 10 and 11 show the dependences of the central pressure $\tilde{p}_0$ on the parameter $\tilde{\Omega}_\infty$. The former shows the curves $\tilde{p}_0(\tilde{\Omega}_\infty)$ for the unexcited Q-ball solutions corresponding to different values of $\tilde{e}$, while the latter shows the curves for the unexcited and first nine radially excited Q-ball solutions for fixed $\tilde{e} = 0.01$. All the curves in Figs. 10 and 11 have similar behavior. They intersect the limiting line $\tilde{\Omega}_\infty = 1$ at the upper and lower points, and possess turning points. The only exception is the curve $\tilde{p}_0(\tilde{\Omega}_\infty)$ in Fig. 10, which corresponds to the nongauged case $\tilde{e} = 0$; this curve has only one intersection
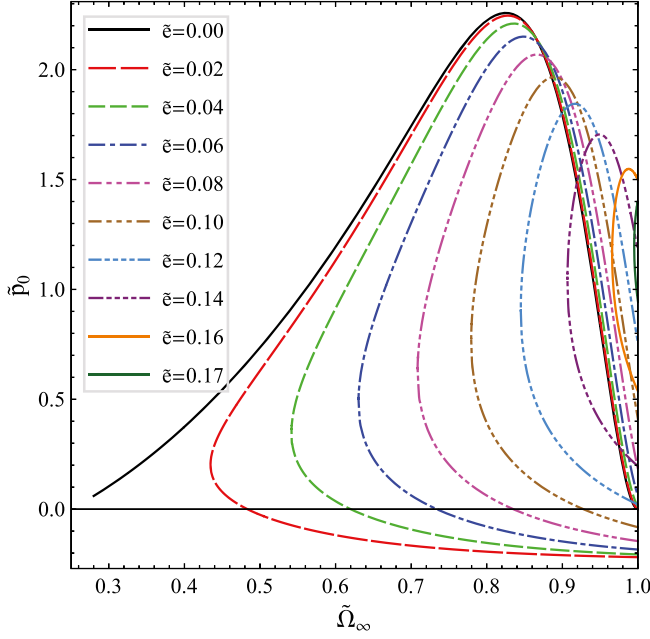
FIG. 10. Curves $\tilde{p}_0(\tilde{\Omega}_\infty)$ for different values of $\tilde{e}$ and $\tilde{h} = 0.2$. The curves correspond to the unexcited Q-ball solution.

point, and does not have a turning point. Note that the positions of the turning points in Figs. 3, 5, and 10 coincide, as do the positions of the turning points in Figs. 4, 8, and 11. However, the main feature of Figs. 10 and 11 is the presence of rather broad intervals of $\tilde{\Omega}_\infty$ in which the central pressure of the Q-ball solution is negative. This behavior is
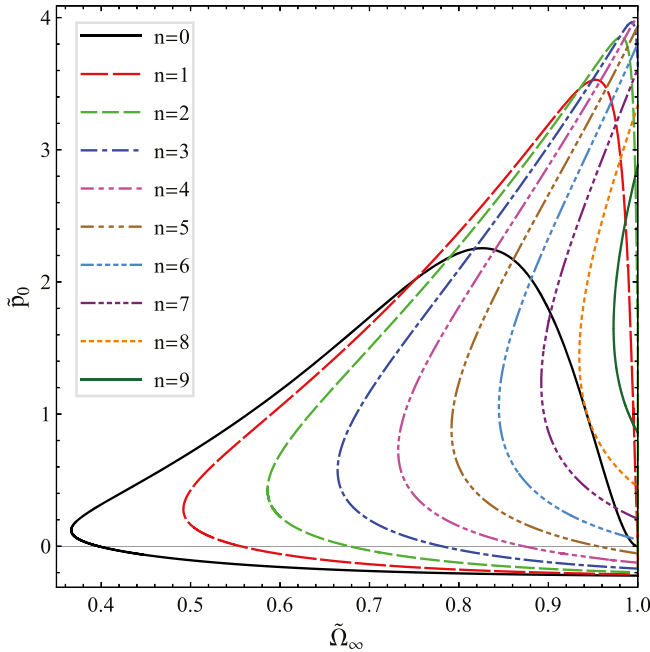

FIG. 11. Curves $\tilde{p}_0(\tilde{\Omega}_\infty)$ for the unexcited and first nine radially excited Q-ball solutions. The curves correspond to parameters $\tilde{e} = 0.01$ and $\tilde{h} = 0.2$.

characteristic for curves corresponding to $\tilde{e} = 0.02$, 0.04, 0.06, 0.08, and 0.1 in Fig. 10 and for the curves corresponding to $n = 0, \ldots, 5$ in Fig. 11. Note that a negative central pressure is characteristic for the quasi-thin-wall regime, i.e., for gauged Q-ball solutions possessing large energies and Noether charges. This is because the central effective potential $\tilde{U}_{\text{eff}}$ (and consequently the central pressure) of large nongauged Q-balls is only slightly higher than zero, and thus may become negative when we turn on the electromagnetic interaction. Finally, of all the curves in Figs. 10 and 11, only the one corresponding to the nongauged Q-ball in Fig. 10 tends to zero at both (left and right) terminal points. This is because the effective potential of the nongauged Q-ball tends to zero in both the thin-wall ($\tilde{\Omega}_\infty \to [1 - (3/16)\tilde{h}^{-1}]^{1/2}$) and thick-wall ($\tilde{\Omega}_\infty \to 1$) regimes.

A detailed description of the forms of the radially excited nongauged Q-ball solutions is given in Ref. [12]. We have found that the forms of the ansatz function $f(r) = mg^{-1/2}\tilde{f}(\tilde{r})$, the energy density $\mathcal{E}(r) = m^4 g^{-1}\tilde{\mathcal{E}}(\tilde{r})$, the Noether charge density $j_N^0(r) = m^3 g^{-1}\tilde{j}_N^0(\tilde{r})$, and the pressure $p(r) = m^4 g^{-1}\tilde{p}(\tilde{r})$ for the gauged case are similar to those for the nongauged case. We give as an example only the excited Q-ball solution shown in Fig. 12, corresponding to the parameters $\tilde{e} = 0.01$, $\tilde{h} = 0.2$, $n = 9$, and $\tilde{\Omega}_\infty = 0.9817$, as it demonstrates all of the characteristic properties of radially excited gauged Q-ball solutions. Note that the solution in Fig. 12 is the maximum possible radially excited solution for a given $\tilde{e}$ and $\tilde{h}$. We can see that the ansatz function $\tilde{f}(\tilde{r})$ has the nine nodes ($n = 9$) that separate the nine alternating peaks. At the same time, the ansatz function $\tilde{\Omega}(\tilde{r})$ increases monotonically on the interval $[0, \infty)$, in accordance with Eq. (16a).
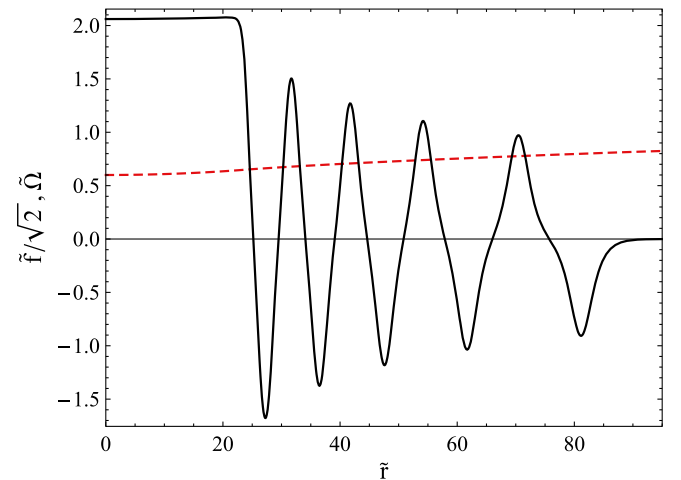

FIG. 12. Profile functions $\tilde{f}(\tilde{r})/\sqrt{2}$ (solid line) and $\tilde{\Omega}(\tilde{r})$ (dashed line) for the ninth ($n = 9$) radially excited Q-ball solution. The solution corresponds to parameters $\tilde{e} = 0.01$, $\tilde{h} = 0.2$, and $\tilde{\Omega}_\infty = 0.9817$.

It was found numerically that for n close to the maximum possible value the absolute values of $\tilde{f}$ at the peak positions $\tilde{r}_i$ approximately satisfy the relation

$$|\tilde{f}(\tilde{r}_i)|\tilde{r}_i^{\frac{1}{2}} \approx \text{const.} \qquad (52)$$

This can be explained as follows. It is shown in Appendix B [see Eqs. (B4) and (B5)] that the system of differential equations (13) and (14) describes the two-dimensional motion of a particle with unit mass in the plane $(\tilde{f}, \tilde{\Omega})$. The particle moves in the force field of the effective potential $\tilde{U}_{\text{eff}}(\tilde{f}) = \tilde{\Omega}^2 \tilde{f}^2/2 - V(\tilde{f})$ and experiences the action of the nonconservative force $\tilde{\mathbf{F}}_{\text{nc}} = (0, (1 + \tilde{e}^2)\tilde{\Omega}\tilde{f}^2)$ and the friction force $\tilde{\mathbf{F}}_{\text{f}} = (-2\tilde{r}^{-1}\tilde{f}', -2\tilde{r}^{-1}\tilde{\Omega}')$. Next, the amplitudes of the peaks in Fig. 12 are determined by the effective potential $\tilde{U}_{\text{eff}}(\tilde{f})$. In the wide neighborhood of the point $(\tilde{f}, \tilde{\Omega}) = (0, 1)$, the contour lines corresponding to zero levels of U_{eff} and $\partial_{\tilde{f}} U_{\text{eff}}$ are well described by the approximate expressions $\tilde{f} \approx 2(1 - \tilde{\Omega})^{1/2}$ and $\tilde{f} \approx 2\sqrt{2}(1 - \tilde{\Omega})^{1/2}$, respectively. During the oscillations, the particle must intersect with the zero level of $\partial_{\tilde{f}} U_{\text{eff}}$; otherwise, there is no restoring force, and oscillations are impossible. At the same time, the "coordinate" $\tilde{f}$ of the particle cannot significantly exceed the zero level of U_{eff}; otherwise, oscillations are also impossible. We see that in the neighborhood of the point $(\tilde{f}, \tilde{\Omega}) = (0, 1)$ the amplitudes of $\tilde{f}$ oscillations are approximately proportional to $(1 - \tilde{\Omega})^{1/2}$. Equation (19) also tells us that in the neighborhood of $\tilde{\Omega} = 1$ the difference $1 - \tilde{\Omega} \propto \tilde{r}^{-1}$. A combination of the last two expressions results in Eq. (52).

Figure 13 shows the distributions of the energy density $\tilde{\mathcal{E}}(\tilde{r})$, the Noether charge density $\tilde{j}_N^0(\tilde{r})$, and the pressure $\tilde{p}(\tilde{r})$ corresponding to the Q-ball solution in Fig. 12. All three distributions consist of a central region, where $\tilde{\mathcal{E}}$, $\tilde{j}_N^0$, and $\tilde{p}$ weakly depend on $\tilde{r}$, followed by a region in which $\tilde{\mathcal{E}}$, $\tilde{j}_N^0$, and $\tilde{p}$ oscillate. However, the oscillation patterns of $\tilde{\mathcal{E}}$, $\tilde{j}_N^0$, and $\tilde{p}$ are different. The Noether charge density $\tilde{j}_N^0(\tilde{r})$ has the simplest oscillation pattern, consisting of a sequence of peaks separated by zero minima. The positions of the zeros in $\tilde{j}_N^0$ coincide with those of the ansatz function $\tilde{f}$, whereas the maxima in $\tilde{j}_N^0$ are slightly different from those of $\tilde{f}$ due to the inconstancy of $\tilde{\Omega}$ in Eq. (23). From Eq. (52), it follows that the height of the ith peak of $\tilde{j}_N^0$ is approximately inversely proportional to its radial position $\tilde{r}_i$, whereas from Fig. 13, it follows that the width of the ith peak increases moderately with an increase in i as well as the distance $\tilde{r}_i - \tilde{r}_{i-1}$ between neighboring peaks.

The pattern of oscillation of the energy density $\tilde{\mathcal{E}}$ is more complicated than that of the Noether charge density $\tilde{j}_N^0$. As in the previous case, it is a sequence of peaks separated by minima, but the peaks have a complicated structure, and the minima are nonzero. For $i \leq 4$, there are small, sharp peaks
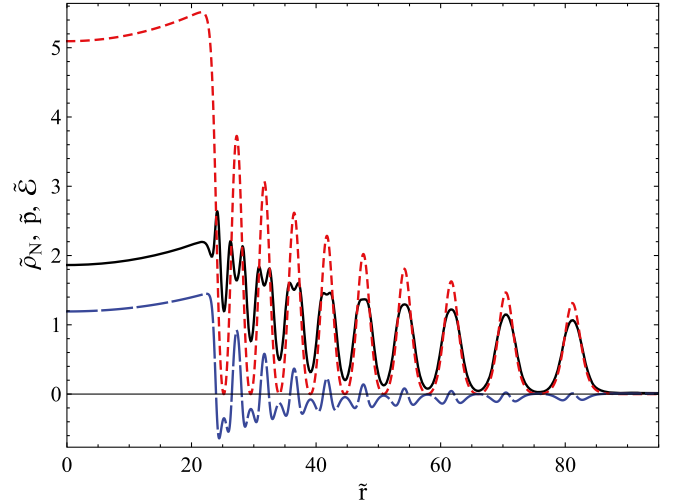

FIG. 13. Energy density $\tilde{\mathcal{E}}(\tilde{r})$ (solid line), Noether charge density $\tilde{\rho}(\tilde{r}) = \tilde{j}_N^0(\tilde{r})$ (short-dashed line), and pressure $\tilde{p}(\tilde{r})$ (long-dashed line) corresponding to the Q-ball solution in Fig. 12.

against a background of wider basic peaks. This complicated pattern of peaks is due to the interference between the gradient (35b), kinetic (35c), and potential (35d) parts of the energy density, where the small, sharp peaks arise from the contribution of the gradient part. With an increase in i, the contribution of the gradient part decreases due to the decrease in the derivative $\tilde{f}'(\tilde{r})$; this results in the disappearance of the small, sharp peaks, starting with $i = 5$. The values of $\tilde{\mathcal{E}}$ at the minimum points located between the wide basic peaks are nonzero and result from the contributions of the electric (35a) and gradient (35b) parts, where the contribution of the latter predominates. These values therefore allow us to estimate the relative contributions of the gradient and electric energy densities to the total energy density.

The oscillation behavior of the pressure $\tilde{p}$ is also rather complicated. Unlike the energy and Noether charge densities, the pressure $\tilde{p}$ may be negative. Indeed, we see that in Fig. 13 the negative minima of $\tilde{p}$ are separated by positive peaks, the positions of which approximately coincide with those of the Noether charge density $\tilde{j}_N^0$; these positive peaks are due to the kinetic term $\tilde{\Omega}^2 \tilde{f}^2/2$ in Eq. (28). The minima in $\tilde{p}$ have a double-well structure resulting from the interference of the last three terms in Eq. (28). The central maxima of these double wells approximately coincide with the zeros in $\tilde{j}_N^0$, whereas the two side minima of the double wells are due to the contribution from the negative gradient term $-\tilde{f}'^2/6$ in Eq. (28).

The solution in Fig. 12 corresponds to the initial values $\tilde{f}_0 = 2.9$ and $\tilde{\Omega}_0 = 0.6$; for a given $\tilde{e}$ and $\tilde{h}$, it has the maximum possible number of nodes ($n = 9$). Note that these initial values satisfy the condition of the quasi-thin-wall regime (48). We also studied radially excited Q-ball

solutions with the same $\tilde{\Omega}_0$ but a smaller number of nodes. All these solutions also satisfy the quasi-thin-wall condition (48), and thus their initial values $\tilde{f}_0$ are very close to that of the solution in Fig. 12. It was found numerically that starting with $n = 4$ the energy and Noether charge of these solutions satisfy the approximate relations

$$\tilde{E}^{1/3} \approx a_{\tilde{E}} + b_{\tilde{E}} n, \qquad \tilde{Q}_N^{1/3} \approx a_{\tilde{Q}_N} + b_{\tilde{Q}_N} n, \quad (53)$$

where the coefficients $a_{\tilde{E}}$, $b_{\tilde{E}}$, $a_{\tilde{Q}_N}$, and $b_{\tilde{Q}_N}$ depend on the position of the initial point $(\tilde{f}_0, \tilde{\Omega}_0)$ on the quasi-thin-wall regime curve (48). Note that the relations (53) are similar to those obtained in Ref. [12] for radially excited nongauged Q-balls. In the latter case, however, the number of radially excited Q-balls is infinite, whereas in the gauged case, it is finite and increases with a decrease in the gauge coupling constant $\tilde{e}$.

V. CONCLUSION

In the present paper, radially excited $U(1)$ gauged Q-balls have been investigated both analytically and numerically. In particular, the domain of existence of $U(1)$ gauged Q-balls in the parameter space has been found by numerical methods. It has also been found that the presence of an Abelian gauge field leads to substantial changes in the properties of radially excited gauged Q-balls compared to nongauged ones. First, there exists only a finite number of radially excited gauged Q-balls at given values of the model's parameters, whereas in the nongauged case, the number of radially excited Q-balls is infinite. For the nth radially excited gauged Q-ball solution, there exist a maximum possible Noether charge and energy, both of which decrease with an increase in n. For a given n, there also exists a maximum allowable value of the gauge coupling constant; there is no nth radially excited gauged Q-ball if the gauge coupling constant exceeds this limiting value. In the same way as the maximum possible Noether charge and energy, the maximum allowable gauge coupling constant decreases with an increase in n. Note that this behavior of the radially excited gauged Q-balls is similar to that of the unexcited one [14,24].

Another characteristic feature of gauged Q-balls (both unexcited and radially excited) is the existence of turning points in the curves describing the dependences of the energy, the Noether charge, and several other quantities on the parameter Ω_∞. All of these turning points are due to the inflection point on the curve $E(Q_N)$ describing the dependence of the energy of the Q-ball on the Noether charge. This inflection point, in turn, results from the long-range nature of the electrostatic Coulomb repulsion.

Unlike nongauged Q-balls, gauged ones (both unexcited and radially excited) may have a negative pressure in the central domain. This behavior holds for the gauged Q-balls with a sufficiently large Noether charge (quasi-thin-wall regime). However, the central pressure of the gauged Q-ball becomes positive with increases in both the gauge coupling constant and the radial excitation.

At a fixed Noether charge, the energy of the gauged Q-ball increases with an increase in the radial excitation (i.e., with an increase in n). It follows that the ith excited gauged Q-ball can transition into less excited Q-balls with $n = 1, ..., i - 1$ or into an unexcited Q-ball with $n = 0$; the energy released is carried away by electromagnetic and scalar waves.

In the present paper, we have considered radially excited gauged Q-balls in three-dimensional space, whereas three-dimensional radially excited nongauged Q-balls were studied in Refs. [10,12]. It is obvious that radially excited nongauged Q-balls also exist in two spatial dimensions and do not exist in one dimension. The existence of radially excited nongauged Q-balls is due to the existence of the "friction" term $(d - 1)f'(r)/r$ in the differential equation for the ansatz function $f(r)$. This term is nonzero in the two-dimensional ($d = 2$) case and vanishes in the one-dimensional ($d = 1$) case, making the existence of one-dimensional radially excited Q-balls impossible.

It is known that one- and two-dimensional electrically charged objects must have infinite electrostatic energy, meaning that the existence of one- and two-dimensional electrically charged solitons in Maxwell gauge models is impossible. Note, however, that two-dimensional electrically charged solitons can exist in gauge models for which the Lagrangians include the Chern-Simons term [31–39]. In Maxwell gauge models, however, there are one- and two-dimensional soliton systems with zero total electric charge but a nonzero electric field [40–42]. These soliton systems are unexcited; however, there are no reasons prohibiting radial (in two spatial dimensions) or linear (in one spatial dimension) excitations for them.

ACKNOWLEDGMENTS

APPENDIX A: TIME INDEPENDENCE OF GAUGED Q-BALL FIELDS IN THE UNITARY GAUGE

To establish the time dependence of the gauged Q-ball, the Hamiltonian formalism can be used together with the Lagrange multipliers method [43,44]. First of all, we must fix the gauge. We shall use the unitary gauge, in which the imaginary part of the complex scalar field vanishes,

$$\text{Re}(\phi) = \frac{f}{\sqrt{2}}, \qquad \text{Im}(\phi) = 0, \qquad (A1)$$

and the Lagrangian density (1) takes the form

$$\mathcal{L} = -\frac{1}{4}F_{\mu\nu}F^{\mu\nu} + \frac{1}{2}\partial_\mu f \partial^\mu f + \frac{e^2}{2}A_\mu A^\mu f^2 - V(f). \quad (A2)$$

Using Eq. (A2), we obtain the generalized momenta corresponding to the fields f, $A_x = A^1$, $A_y = A^2$, and $A_z = A^3$,

$$\Pi_f = \frac{\partial \mathcal{L}}{\partial(\partial_t \phi_1)} = \partial_t f, \quad (A3a)$$

$$\Pi_{A_x} = \frac{\partial \mathcal{L}}{\partial(\partial_t A_x)} = F_{10} = -E_x, \quad (A3b)$$

$$\Pi_{A_y} = \frac{\partial \mathcal{L}}{\partial(\partial_t A_y)} = F_{20} = -E_y, \quad (A3c)$$

$$\Pi_{A_z} = \frac{\partial \mathcal{L}}{\partial(\partial_t A_z)} = F_{30} = -E_z, \quad (A3d)$$

and the Hamiltonian density

$$\begin{aligned}
\mathcal{H} &= \partial_t f \Pi_f + \partial_t A_x \Pi_{A_x} + \partial_t A_y \Pi_{A_y} + \partial_t A_z \Pi_{A_z} - \mathcal{L} \\
&= \frac{1}{2}\Pi_{A_x}^2 + \frac{1}{2}\Pi_{A_y}^2 + \frac{1}{2}\Pi_{A_z}^2 + \frac{1}{2}\Pi_f^2 + \frac{1}{4}F_{ij}F_{ij} \\
&\quad + \frac{1}{2}(\partial_x f)^2 + \frac{1}{2}(\partial_y f)^2 + \frac{1}{2}(\partial_z f)^2 \\
&\quad - \frac{e^2}{2}f^2(A_0^2 - A_x^2 - A_y^2 - A_z^2) \\
&\quad - \Pi_{A_x}\partial_x A_0 - \Pi_{A_y}\partial_y A_0 - \Pi_{A_z}\partial_z A_0 + V(f), \quad (A4)
\end{aligned}$$

where we express the time derivatives of the fields in terms of the generalized momenta.

Since the Hamiltonian density (A4) does not depend on the derivative $\partial_t A_0$, we have the primary constraint $\Pi_{A_0} = 0$. The primary constraint must hold at any instant of time, and thus the Poisson bracket of the generalized momentum Π_{A_0} with the Hamiltonian $H = \int \mathcal{H}d^3x$ must vanish. This condition leads us to the secondary constraint

$$\frac{\delta H}{\delta A_0} = \partial_x \Pi_{A_x} + \partial_y \Pi_{A_y} + \partial_z \Pi_{A_z} - e^2 f^2 A_0 = 0. \quad (A5)$$

Taking into account the expression for the electric charge density in the unitary gauge, $\rho = j_0 = -e^2 f^2 A_0$, and the definitions of the generalized momenta in Eqs. (A3b)–(A3d), we see that constraint (A5) is Gauss's law

$$\partial_i E_i = \rho. \quad (A6)$$

Gauss's law makes it possible to represent the Noether charge of a field configuration of the model as the surface integral of the flux of the generalized momenta:

$$\begin{aligned}
Q_N &= e^{-1}\int \rho d^3x = -e^{-1}\int \partial_i \Pi_{A^i}d^3x \\
&= -e^{-1}\oint_{S_\infty} \Pi_{A^i}dS_i. \quad (A7)
\end{aligned}$$

The energy density $\mathcal{E} = T_{00}$ can also be expressed in terms of the generalized momenta and the corresponding fields

$$\begin{aligned}
\mathcal{E} &= \frac{1}{2}\Pi_{A_x}^2 + \frac{1}{2}\Pi_{A_y}^2 + \frac{1}{2}\Pi_{A_z}^2 + \frac{1}{2}\Pi_f^2 + \frac{1}{4}F_{ij}F_{ij} \\
&\quad + \frac{1}{2}(\partial_x f)^2 + \frac{1}{2}(\partial_y f)^2 + \frac{1}{2}(\partial_z f)^2 \\
&\quad + \frac{e^2}{2}f^2(A_0^2 + A_x^2 + A_y^2 + A_z^2) + V(f). \quad (A8)
\end{aligned}$$

We see that the energy density (A8) does not coincide with the Hamiltonian density (A4):

$$\mathcal{E} - \mathcal{H} = \Pi_{A_x}\partial_x A_0 + \Pi_{A_y}\partial_y A_0 + \Pi_{A_z}\partial_z A_0 + e^2 A_0^2 f^2. \quad (A9)$$

However, after integrating by parts, the right-hand side of Eq. (A9) vanishes for field configurations which have finite energy (so $\lim_{r\to 0}\Pi_{A^i} = 0$) and satisfy Gausss law (A5), and hence for these field configurations,

$$E = \int \mathcal{E}d^3x = H = \int \mathcal{H}d^3x. \quad (A10)$$

It can be shown that in the unitary gauge the field equations (6) and (7) can be written in the Hamiltonian form,

$$\partial_t \Pi_f = -\frac{\delta H}{\delta f} = -\frac{\delta E}{\delta f}, \qquad \partial_t \Pi_{A^i} = -\frac{\delta H}{\delta A^i} = -\frac{\delta E}{\delta A^i}, \quad (A11)$$

where Eq. (A10) is used. When calculating the variational derivatives in Eq. (A11), the time component A_0 of the electromagnetic potential must be expressed in terms of the canonical variables f and Π_{A^i} using Gauss's law (A5):

$$A_0 = e^{-2}f^{-2}(\partial_x \Pi_{A_x} + \partial_y \Pi_{A_y} + \partial_z \Pi_{A_z}). \quad (A12)$$

The remaining Hamilton equations

$$\partial_t f = \frac{\delta E}{\delta \Pi_f} = \frac{\delta H}{\delta \Pi_f}, \qquad \partial_t A^i = \frac{\delta E}{\delta \Pi_{A_i}} = \frac{\delta H}{\delta \Pi_{A^i}} \quad (A13)$$

are simply the definitions of the generalized momenta (A3a)–(A3d). Next, from Eq. (10), it follows that in the Q-ball field configuration the variation in the energy $\delta E = \lambda \delta Q_N$, where λ is the Lagrange multiplier. In deriving

the field equations (A11) and (A13), we must consider only those variations of fields and generalized momenta that vanish at spatial infinity. In particular, $\delta\Pi_{A^i}|_{S_\infty} = 0$, so from Eq. (A7), it follows that $\delta Q_N = 0$ for these variations. Since $\delta E = \lambda \delta Q_N$ in the Q-ball field configuration, the variation δE also vanishes. It then follows from Eqs. (A11) and (A13) that the fields f and A^i and the corresponding generalized momenta Π_f and Π_{A^i} do not depend on time in the unitary gauge. The time component A_0 of the electromagnetic potential also does not depend on time in the unitary gauge, as this follows from Eq. (A12). Note, however, that Eq. (10) also holds for variations in the fields and generalized momenta that lead to nonzero δE and δQ_N. In particular, it holds for variations connecting two infinitesimally close Q-ball field configurations, giving rise to the differential relation (11).

Now, let us investigate how the Lagrange multiplier λ is related to the parameters of the gauged Q-ball. To do this, we shall follow the method of Ref. [21]. First, note that in the unitary gauge the electromagnetic potential A_0 of the gauged Q-ball must tend to some constant value; otherwise, the energy of the gauged Q-ball would be infinite. Let us denote this limiting value of $A_0(r)$ as $-e^{-1}\bar{\lambda}$; then, the combination $\Omega(r) = -eA_0(r)$ can be represented as

$$\Omega(r) = \bar{\Omega}(r) + \bar{\lambda}, \tag{A14}$$

where $\lim_{r\to\infty}\bar{\Omega}(r) = 0$. Using Eqs. (23), (24), and (A14), we obtain expressions for derivatives of the Noether charge Q_N and the energy E of the gauged Q-ball with respect to $\bar{\lambda}$,

$$\frac{dQ_N}{d\bar{\lambda}} = 4\pi \int_0^\infty \left(f^2\left(1 + \frac{d\bar{\Omega}}{d\bar{\lambda}}\right) + 2f\frac{df}{d\bar{\lambda}}(\bar{\Omega} + \bar{\lambda}) \right) r^2 dr, \tag{A15}$$

$$\frac{dE}{d\bar{\lambda}} = 4\pi \int_0^\infty \left(e^{-2}\bar{\Omega}'\left(\frac{d\bar{\Omega}}{d\bar{\lambda}}\right)' + f'\left(\frac{df}{d\bar{\lambda}}\right)' \right.$$
$$+ f^2(\bar{\Omega} + \bar{\lambda})\left(1 + \frac{d\bar{\Omega}}{d\bar{\lambda}}\right)$$
$$\left. + f\frac{df}{d\bar{\lambda}}(\bar{\Omega} + \bar{\lambda})^2 + \frac{dV}{df}\frac{df}{d\bar{\lambda}} \right) r^2 dr, \tag{A16}$$

where the prime means differentiation with respect to the radial variable r. Next, we integrate the term $f'(df/d\bar{\lambda})'r^2$ in Eq. (A16) by parts and use Eqs. (13), (15), and (A15) to recast Eq. (A16) in the form

$$\frac{dE}{d\bar{\lambda}} = \bar{\lambda}\frac{dQ_N}{d\bar{\lambda}} + 4\pi \int_0^\infty \left(e^{-2}\bar{\Omega}'\left(\frac{d\bar{\Omega}}{d\bar{\lambda}}\right)' \right.$$
$$\left. + \bar{\Omega}\left(f^2\left(1 + \frac{d\bar{\Omega}}{d\bar{\lambda}}\right) + 2f\frac{df}{d\bar{\lambda}}(\bar{\Omega} + \bar{\lambda}) \right) \right) r^2 dr. \tag{A17}$$

We can then use Eq. (A14) and differentiate Eq. (14) with respect to $\bar{\lambda}$ to obtain the relation

$$\left(\frac{d\bar{\Omega}}{d\bar{\lambda}}\right)'' + \frac{2}{r}\left(\frac{d\bar{\Omega}}{d\bar{\lambda}}\right)' - e^2 f^2\left(1 + \frac{d\bar{\Omega}}{d\bar{\lambda}}\right)$$
$$- 2e^2 f\frac{df}{d\bar{\lambda}}(\bar{\Omega} + \bar{\lambda}) = 0. \tag{A18}$$

We now integrate the term $e^{-2}\bar{\Omega}'(d\bar{\Omega}/d\bar{\lambda})'r^2$ in Eq. (A17) by parts and use Eq. (A18) to show that in Eq. (A17) the integral term vanishes for the Q-ball field configuration. Thus, $dE/d\bar{\lambda} = \bar{\lambda}dQ_N/d\bar{\lambda}$, and as a consequence, we obtain the relation

$$\frac{dE}{dQ_N} = \bar{\lambda}. \tag{A19}$$

From Eqs. (11) and (A19), it follows that $\lambda = \bar{\lambda}$, and we conclude that in the unitary gauge the Lagrange multiplier $\lambda = -eA_0^\infty$, where A_0^∞ is $\lim_{r\to\infty} A_0(r)$.

We have shown that the gauge Q-ball solution does not depend on time in the unitary gauge. Of course, this time independence is not gauge invariant. In particular, under the gauge transformations (3) with the gauge function $\Lambda(\mathbf{x}, t) = e^{-1}\omega t$, the unitary Q-ball solution (9) becomes the gauge transformed solution

$$\phi^\omega(r, t) = f(r)\exp(-i\omega t), \tag{A20a}$$

$$A_0^\omega(r) = A_0(r) + e^{-1}\omega, \tag{A20b}$$

which depends on t. At the same time, the combination $\Omega^\omega(r) = \omega - eA_0^\omega(r)$ does not depend on the gauge parameter ω and thus coincides with the unitary gauge combination $\Omega(r) = -eA_0(r)$. In particular, it follows from Eq. (A20b) that $\Omega_\infty = \lim_{r\to\infty}\Omega^\omega(r)$ is equal to the Lagrange multiplier λ,

$$\Omega_\infty = \lim_{r\to\infty}(\omega - eA_0^\omega(r))$$
$$= -e\lim_{r\to\infty}A_0(r) = -eA_0^\infty = \lambda, \tag{A21}$$

and thus the differential relation (11) can be written in the form

$$\frac{dE}{dQ_N} = \Omega_\infty, \tag{A22}$$

which is valid for an arbitrary gauge parameter ω. Note that if $\lim_{r\to\infty} A_0^\omega(r) = 0$ (this gauge is often used to describe gauged Q-balls) then $\Omega_\infty = \omega$ and Eq. (A22) takes the form $dE/dQ_N = \omega$.

APPENDIX B: EXISTENCE OF A MAXIMUM POSSIBLE ELECTRIC CHARGE FOR GAUGED Q-BALLS

It is known that in most cases the electric charge of a gauged Q-ball cannot be arbitrarily large. It was pointed out in Ref. [20] that this situation arises when the second derivative of the self-interaction potential $d^2V(|\phi|)/d|\phi|^2$ is finite at $|\phi| = 0$. We will discuss this point in more detail. Multiplying Eq. (14) by r and integrating by parts, we obtain the integral relation $\int_0^\infty \Omega'(r)dr = e\int_0^\infty rj_0(r)dr$, which implies that

$$\Delta\Omega = \Omega_\infty - \Omega_0 = e\int_0^\infty rj_0(r)dr. \qquad (B1)$$

On the other hand, Eqs. (16a), (20), (21), and (22) lead us to the conclusion

$$\Delta\Omega < \Omega_\infty \le m, \qquad (B2)$$

where we assume for definiteness that the parameter Ω_∞ is positive. Equations (B1) and (B2) result in the inequality

$$e\int_0^\infty rj_0(r)dr < m, \qquad (B3)$$

where for field models with regular self-interaction potentials the squared mass $m^2 = 2^{-1}d^2V(|\phi|)/d|\phi|^2$ at $|\phi| = 0$.

We now show that Eq. (B3) cannot be satisfied if the gauged Q-ball can possess an arbitrarily large electric charge $Q = 4\pi\int_0^\infty r^2 j_0(r)dr$. First, it should be noted that the electric charge density $j_0(r) = e\Omega(r)f(r)^2$ is a bounded function of r. Indeed, from Eq. (16), it follows that $\Omega(r) \in (0, m]$ and thus is bounded. At the same time, it can be shown that, regardless of the value of r, the ansatz function $f(r)$ cannot exceed the limiting value $\sqrt{2g/h}$; otherwise, the term $(\Omega^2 - m^2)f + gf^3/2 - hf^5/4$ in Eq. (13) is negative for $\Omega \in (0, m]$, and thus $f(r)$ increases indefinitely. The boundary condition $f(r) \xrightarrow{r\to\infty} 0$ is therefore not met, and the gauged Q-ball does not exist. We can conclude that the electric charge density of the gauged Q-ball is bounded on the interval $r \in [0, \infty)$.

Now, we consider the possible variants of the electric charge density $j_0(r)$ that lead to an arbitrarily large electric charge $Q = 4\pi\int_0^\infty j_0(r)r^2dr$. The first variant corresponds to the case when the integral $I = \int_0^\infty j_0(r)dr$ is infinite. In this case, however, the integral $J = \int_0^\infty rj_0(r)dr$

is also infinite, and thus Eq. (B3) cannot be satisfied. Consequently, this variant of $j_0(r)$ cannot be realized.

The second variant of $j_0(r)$ corresponds to the case when the integral $I = \int_0^\infty j_0(r)dr$ is finite but the electric charge $Q = 4\pi\int_0^\infty j_0(r)r^2dr$ is infinite. Note in this connection that Eqs. (20)–(22) lead to the conclusion that the electric charge density $j_0(r) = e\Omega(r)f(r)^2$ tends to zero exponentially as $r \to \infty$. It follows that the electric charge Q cannot have an infinite contribution from the spatial asymptotics of $j_0(r)$. If we suppose that the maximum of $j_0(r)$ does not tend to zero, then this means that the electric charge density is localized within a finite vicinity of this maximum, and the radial position of the maximum increases indefinitely. Using the mean value theorem, we find that for this electric charge density $Q \sim R^2$ and $J \sim R$, where R is the radial position of the maximum of $j_0(r)$. We see that an indefinite increase in Q leads to an indefinite increase in R, and as a consequence to an indefinite increase in the integral $J = \int_0^\infty rj_0(r)dr$. Because of this, Eq. (B3) again cannot be satisfied, and this variant of $j_0(r)$ is also unrealizable.

There is one more possible variant, which corresponds to the case where the electric charge density $j_0(r)$ spreads over the semi-infinite interval $r \in [0, \infty)$ in such a way that the integral I tends to zero while the electric charge Q increases indefinitely. In this case, the integral $J = \int_0^\infty rj_0(r)dr$ may be finite, and condition (B3) may be met. However, since the integral $I = \int_0^\infty j_0(r)dr$ tends to zero, the maximum of $j_0(r)$ also tends to zero, and consequently so does the maximum of the ansatz function $f(r)$. We now show that this behavior of $f(r)$ cannot be realized. First, note that the system of differential equations (13) and (14) can be represented in the form

$$f'' + \frac{2}{r}f' = -\frac{\partial}{\partial f}U_{\rm eff}(f, \Omega), \qquad (B4a)$$

$$\Omega'' + \frac{2}{r}\Omega' = -\frac{\partial}{\partial\Omega}U_{\rm eff}(f, \Omega) + (1 + e^2)\Omega f^2, \qquad (B4b)$$

where the effective potential

$$U_{\rm eff}(f, \Omega) = \frac{1}{2}(\Omega^2 - m^2)f^2 + \frac{g}{8}f^4 - \frac{h}{24}f^6. \qquad (B5)$$

The system (B) describes the two-dimensional motion of a particle with unit mass in the plane (f, Ω), where the radial variable r plays the role of time. The particle moves in a viscous medium under the action of a conservative force $\mathbf{F}_{\rm c} = (-\partial_f U_{\rm eff}, -\partial_\Omega U_{\rm eff})$, a nonconservative force $\mathbf{F}_{\rm nc} = (0, (1 + e^2)\Omega f^2)$, and a friction force $\mathbf{F}_{\rm f} = (-2r^{-1}f', -2r^{-1}\Omega')$, which is also nonconservative.

The structure of the level lines of the effective potential $U_{\rm eff}(f, \Omega)$ leads to the conclusion that the particle must start moving in the close vicinity of the point $(0, m)$ in order

to have the infinitesimal coordinate $f(r)$. In this case, the initial coordinate Ω_0 satisfies the condition

$$m^2 - \Omega_0^2 \equiv \mu^2 \ll m^2, \qquad (B6)$$

from which it follows that

$$\Delta\Omega = \Omega_\infty - \Omega_0 < m - \Omega_0 \approx \frac{\mu^2}{2m}. \qquad (B7)$$

We now estimate the effective radial size ΔR of the electric charge distribution for this case. From Eq. (B4a), it follows that the motion of the particle along the coordinate f is determined by the action of the force $-\partial_f U_{\mathrm{eff}}$. The effective potential U_{eff} is negative in the interval $f \in (0, 2g^{-1/2}\mu)$ and has a local minimum at $f_{\min} = 2^{1/2}g^{-1/2}\mu$, where condition (B6) is used. In the neighborhood of the local minimum $f_{\min}$, the effective potential U_{eff} takes the form

$$U_{\mathrm{eff}} \approx -\frac{\mu^4}{2g} + \mu^2 \left(f - \sqrt{\frac{2}{g}}\mu\right)^2, \qquad (B8)$$

and thus in the neighborhood of $f_{\min}$, the motion of the particle is harmonic with period $T = \sqrt{2}\pi/\mu$. We can use the period T to estimate ΔR. In doing so, we neglect the friction force $-2r^{-1}f'$ and the nonharmonic nature of the effective potential U_{eff} and assume that the coordinate Ω is fixed when the particle moves along the coordinate f. All these factors, however, can only result in an increase in the effective radial size ΔR, and thus we have the estimation

$$\Delta R > a\mu^{-1}, \qquad (B9)$$

where a is a finite positive constant. To estimate the value of the ansatz function f on the interval ΔR, we note that the minimum point $f_{\min} = 2^{1/2}g^{-1/2}\mu$ and the nearest zero point $f = 2g^{-1/2}\mu$ of the effective potential U_{eff} are both of the order μ. Hence, the particle moving in the force field of the effective potential U_{eff} will have the coordinate f of the order μ on the "time" interval ΔR, and we obtain the estimation

$$f > b\mu, \qquad (B10)$$

where b is a finite positive constant. Equations (16a) and (B10) lead to an estimation for the electric charge density j_0 on the interval ΔR,

$$j_0 > e\Omega_0 b^2 \mu^2. \qquad (B11)$$

We can now obtain an estimation for the integral J,

$$J = \int_0^\infty r j_0(r)dr = \int_0^{\Delta R} r j_0(r)dr + A$$

$$> e\Omega_0 b^2 \mu^2 \int_0^{\Delta R} r\,dr + A > \frac{1}{2}e\Omega_0 a^2 b^2, \qquad (B12)$$

where we use the fact that the integral $A = \int_{\Delta R}^\infty r j_0(r)dr$ is finite, since from Eqs. (20)–(22) it follows that $j_0(r)$ tends to zero exponentially as $r \to \infty$. In the same way, it can be shown that the integral J is less than some positive finite value. Hence, the integral J is finite as $\mu \to 0$. On the other hand, Eqs. (23), (B9), and (B11) result in a lower estimation for the electric charge Q:

$$Q > \frac{4\pi}{3}e\Omega_0 a^3 b^2 \mu^{-1}. \qquad (B13)$$

Thus, the integral J is finite, whereas the electric charge Q increases indefinitely as $\mu \to 0$. At the same time, Eq. (B7) tells us that $\Delta\Omega < \mu^2/(2m)$ and therefore vanishes as $\mu \to 0$. It follows that the condition $\Delta\Omega = eJ$ [Eq. (B1)] does not hold as $\mu \to 0$, and thus a gauged Q-ball with an arbitrarily large electric charge cannot exist in this case.

We have shown that gauged Q-balls with arbitrarily large electric charges cannot exist in model (1). The reason lies in the constraint $\Omega_\infty \leq m$, from which it follows that the difference $\Delta\Omega = \Omega_\infty - \Omega_0 < m$. Because of this last inequality, Eq. (B1) can not be satisfied for sufficiently large electric charges, and thus the corresponding Q-balls do not exist.

The regular self-interaction potential $V(|\phi|)$ must have a finite second-order derivative $d^2V(|\phi|)/d|\phi|^2$ at $|\phi| = 0$, and thus the mass m of the complex scalar field ϕ is also finite in this case, since $m^2 = 2^{-1}d^2V(|\phi|)/d|\phi|^2$ at $|\phi| = 0$. The difference $\Delta\Omega = \Omega_\infty - \Omega_0$ therefore remains bounded for all Q-balls with regular self-interaction potentials, and hence such Q-balls cannot possess arbitrarily large electric charges. It follows that there is a maximum allowable electric charge for a gauged Q-ball with a regular self-interaction potential. However, as shown in Refs. [18,20], gauged Q-balls also exist in models where the self-interaction potentials are not regular at $|\phi| = 0$. In particular, the second order derivative $d^2V(|\phi|)/d|\phi|^2$ diverges as $|\phi| \to 0$, and thus there is no upper bound on the difference $\Delta\Omega = \Omega_\infty - \Omega_0$ in these models. This results in the existence of gauged Q-balls with arbitrarily large electric charges [18,20].

Another consequence of Eq. (B3) is that gauged Q-balls cannot exist if the gauge coupling constant e exceeds some upper bound. Indeed, Eq. (B3) cannot be satisfied for sufficiently large e, since, as shown above, the integral $J = \int_0^\infty r j_0(r)dr$ cannot be arbitrarily small. Radially excited gauged Q-balls also cannot exist if the number of nodes n of the ansatz function $f(r)$ increases indefinitely. In this case, the integral $J = \int_0^\infty r j_0(r)dr$ also increases indefinitely, and Eq. (B3) cannot be satisfied. Hence, there is only

a finite number of radially excited gauged Q-balls at given values of the models parameters.

APPENDIX C: EXISTENCE OF AN INFLECTION POINT ON THE CURVE $E(Q_N)$ IN THE GAUGED CASE

In the present paper, the curves in Figs. 3, 4, 5, 8, 10, and 11 have turning points at certain values of the parameter Ω_∞. The existence of these turning points results from the existence of inflection points on the corresponding curves $E(Q_N)$. Indeed, by definition, the second derivative $d^2E/dQ_N^2 = 0$ at an inflection point; the basic relation (11) then tells us that the derivatives $d\Omega_\infty/dQ_N$ and $d\Omega_\infty/dE$ also vanish at the inflection point. Hence, the derivatives $dQ_N/d\Omega_\infty$ and $dE/d\Omega_\infty$ are infinite at the inflection point, resulting in the turning points shown in Figs. 5 and 8. Next, we differentiate Eq. (B1) with respect to the parameter Ω_∞. Taking into account that at the turning point the infinite derivative $dQ_N/d\Omega_\infty$ results from the infinite derivative $\partial j_0/\partial \Omega_\infty$, we conclude that the derivative $d\Omega_0/d\Omega_\infty$ becomes infinite at the turning point in accordance with Figs. 3 and 4. Finally, keeping in mind that the central pressure $p_0 = \Omega_0^2 f_0^2/2 - V(f_0)$, we conclude that the derivative $dp_0/d\Omega_\infty$ is also infinite at the turning point, which is consistent with Figs. 10 and 11.

Combining Eqs. (11) and (41), we obtain the differential relation

$$\frac{dE}{dQ_N} - \frac{E}{Q_N} + \frac{2}{3Q_N}(E^{(G)} - E^{(E)}) = 0. \qquad (C1)$$

From this equation, it follows that if we know how the electric and gradient parts of the energy depend on the Noether charge Q_N, we can determine the dependence of the total energy E of the Q-ball solution on the Noether charge Q_N. In this case, Eq. (C1) becomes a first-order linear inhomogeneous differential equation that can be solved by the method of variation of constants. Of course, the exact forms of the dependences $E^{(E)}(Q_N)$ and $E^{(E)}(Q_N)$ are unknown; however, we can guess the main features of these dependences for sufficiently large Q_N when the interior part and the edge of the Q-ball solution are clearly distinguishable. The electrostatic energy of a compact object possessing the Noether charge Q_N can be written as $E^{(E)}(Q_N) = \alpha Q_N^2/(2R(Q_N))$, where $R(Q_N)$ is the object's effective charge radius, which depends on Q_N, and $\alpha = e^2/(4\pi)$ is the fine-structure constant. For a uniform distribution of the electric charge, the effective charge radius $R \propto Q_N^{1/3}$. If the electric charge is concentrated in the spherical shell of radius R and thickness Δ, then the effective charge radius $R \propto Q_N^{1/2}$. For a gauged Q-ball, we have an intermediate situation and therefore expect that $R \approx \varrho Q_N^\gamma$, where ϱ is a positive constant and the

exponent $\gamma \in (1/3, 1/2)$. Thus, the electrostatic energy of the Q-ball solution is written as

$$E^{(E)}(Q_N) \approx \frac{\alpha}{2\varrho} Q_N^{2-\gamma} \equiv aQ_N^{2-\gamma}. \qquad (C2)$$

Next, we suppose that for sufficiently large Q_N the main contribution to the gradient energy $E^{(G)}$ comes from the edge region of the Q-ball. In this case, the gradient energy of the Q-ball solution takes the form

$$E^{(G)}(Q_N) \approx 4\pi R^2 T = 4\pi \varrho^2 T Q_N^{2\gamma} \equiv bQ_N^{2\gamma}, \qquad (C3)$$

where T is the surface tension.

Substituting Eqs. (C2) and (C3) into Eq. (C1), we obtain a first-order linear inhomogeneous differential equation that can be integrated by the method of variation of constants. The solution to this differential equation can be written as

$$E = cQ_N + \frac{2}{3}\frac{aQ_N^{2-\gamma}}{(1-\gamma)} + \frac{2}{3}\frac{bQ_N^{2\gamma}}{(1-2\gamma)}, \qquad (C4)$$

where c is the integration constant. Note that from Eq. (C4) it follows that the positive constant γ should be less than $1/2$; otherwise, the last term in Eq. (C4) becomes negative or diverges, which is unacceptable from a physical point of view. Under this condition, all the exponents in Eq. (C4) are positive. Next, using Eq. (C4), we obtain the first and second derivatives of the Q-ball's energy with respect to the Noether charge:

$$\frac{dE}{dQ_N} = c + \frac{2}{3}\frac{a(2-\gamma)Q_N^{1-\gamma}}{(1-\gamma)} + \frac{4}{3}\frac{b\gamma Q_N^{2\gamma-1}}{(1-2\gamma)}, \qquad (C5)$$

$$\frac{d^2E}{dQ_N^2} = \frac{2}{3}a(2-\gamma)Q_N^{-\gamma} - \frac{4}{3}b\gamma Q_N^{2\gamma-2}. \qquad (C6)$$

By equating the second derivative (C6) to zero, we obtain the value of the Noether charge at the inflection point:

$$Q_{N,\text{infl}} = \left(\frac{2b\gamma}{a(2-\gamma)}\right)^{\frac{1}{2-3\gamma}}. \qquad (C7)$$

Formally, the existence of the inflection point is related to the fact that the two terms in Eq. (C6) have opposite signs. This is because the exponent $2-\gamma$ in Eq. (C2) is larger than the exponent 2γ in Eq. (C3), due to the multiplier Q_N^2 in the electrostatic energy $E^{(E)}$. In turn, the multiplier Q_N^2 is a consequence of the long-range nature of the electrostatic Coulomb repulsion. Thus, it can be said that the existence of the inflection point is due to the long-range Coulomb repulsion. Indeed, from Eq. (C7), it follows that

$Q_{N,\text{infl}} \propto e^{-2/(2-3\gamma)}$. Hence, $Q_{N,\text{infl}} \to \infty$ as $e \to 0$, which is equivalent to the absence of an inflection point at zero e when there is no Coulomb repulsion.

As mentioned above, the derivative dE/dQ_N cannot exceed the mass m of the scalar ϕ-boson. However, Eq. (C5) tells us that $dE/dQ_N \to \infty$ as $Q_N \to 0$. Hence, Eq. (C4) becomes inapplicable for sufficiently small Q_N. In particular, it does not reproduce the cusp at the minimum possible Q_N. This is because the partition of the Q-ball into an interior and an edge is unclear for small enough Q_N, and thus Eqs. (C2) and (C3) become inapplicable in this case.

When Q_N reaches the maximum possible value $Q_{N,\text{max}}$, the derivative $dE/dQ_N = m$. Combining this result with

Eq. (C5) allows us to express the parameter c in terms of $Q_{N,\text{max}}$ and the rest of the parameters:

$$c = m - \frac{2a}{3}\frac{2-\gamma}{1-\gamma}Q_{N,\text{max}}^{1-\gamma} - \frac{4}{3}\frac{b\gamma}{(1-2\gamma)}Q_{N,\text{max}}^{-1+2\gamma}. \quad \text{(C8)}$$

Finally, note that Eqs. (C2) and (C3) can be considered as an approximation that is only valid for sufficiently large Q_N. In particular, a more accurate description can be achieved if the parameters ϱ and T in Eqs. (C2) and (C3) are some functions of Q_N. Nevertheless, we believe that the simplified approach used here clearly shows the reason for the existence of the inflection point on the curve $E(Q_N)$ in the gauged case.

[1] N. Manton and P. Sutclffe, *Topological Solitons* (Cambridge University Press, Cambridge, England, 2004).
[2] T. D. Lee and Y. Pang, Phys. Rep. **221**, 251 (1992).
[3] G. Rosen, J. Math. Phys. (N.Y.) **9**, 996 (1968).
[4] R. Friedberg, T. D. Lee, and A. Sirlin, Phys. Rev. D **13**, 2739 (1976).
[5] S. Coleman, Nucl. Phys. **B262**, 263 (1985).
[6] A. Safian, S. Coleman, and M. Axenides, Nucl. Phys. **B297**, 498 (1988).
[7] A. Safian, Nucl. Phys. **B304**, 403 (1988).
[8] F. P. Correia and M. Schmidt, Eur. Phys. J. C **21**, 181 (2001).
[9] G. H. Derrick, J. Math. Phys. (N.Y.) **5**, 1252 (1964).
[10] M. S. Volkov and E. Wöhnert, Phys. Rev. D **66**, 085003 (2002).
[11] B. Kleihaus, J. Kunz, and M. List, Phys. Rev. D **72**, 064002 (2005).
[12] M. Mai and P. Schweitzer, Phys. Rev. D **86**, 096002 (2012).
[13] G. Rosen, J. Math. Phys. (N.Y.) **9**, 999 (1968).
[14] K. Lee, J. A. Stein-Schabes, R. Watkins, and L. M. Widrow, Phys. Rev. D **39**, 1665 (1989).
[15] C. H. Lee and S. U. Yoon, Mod. Phys. Lett. A **06**, 1479 (1991).
[16] K. N. Anagnostopoulos, M. Axenides, E. G. Floratos, and N. Tetradis, Phys. Rev. D **64**, 125006 (2001).
[17] T. S. Levi and M. Gleiser, Phys. Rev. D **66**, 087701 (2002).
[18] H. Arodz and J. Lis, Phys. Rev. D **79**, 045002 (2009).
[19] V. Benci and D. Fortunato, J. Math. Phys. (N.Y.) **52**, 093701 (2011).
[20] T. Tamaki and N. Sakai, Phys. Rev. D **90**, 085022 (2014).
[21] I. E. Gulamov, E. Y. Nugaev, and M. N. Smolyakov, Phys. Rev. D **89**, 085006 (2014).
[22] Y. Brihaye, V. Diemer, and B. Hartmann, Phys. Rev. D **89**, 084048 (2014).

[23] J.-P. Hong, M. Kawasaki, and M. Yamada, Phys. Rev. D **92**, 063521 (2015).
[24] I. E. Gulamov, E. Y. Nugaev, A. G. Panin, and M. N. Smolyakov, Phys. Rev. D **92**, 045011 (2015).
[25] M. von Laue, Ann. Phys. (Leipzig) **340**, 524 (1911).
[26] I. Bialynicki-Birula, Phys. Lett. A **182**, 346 (1993).
[27] *Maple User Manual* (Maplesoft, Waterloo, Canada, 2019).
[28] A. G. Panin and M. N. Smolyakov, Phys. Rev. D **95**, 065006 (2017).
[29] R. Friedberg and T. D. Lee, Phys. Rev. D **15**, 1694 (1977).
[30] T. D. Lee and Y. Pang, Nucl. Phys. **B315**, 477 (1989).
[31] S. K. Paul and A. Khare, Phys. Lett. B **174**, 420 (1986).
[32] A. Khare and S. Rao, Phys. Lett. B **227**, 424 (1989).
[33] A. Khare, Phys. Lett. B **255**, 393 (1991).
[34] J. Hong, Y. Kim, and P. Y. Pac, Phys. Rev. Lett. **64**, 2230 (1990).
[35] R. Jackiw and E. J. Weinberg, Phys. Rev. Lett. **64**, 2234 (1990).
[36] R. Jackiw, K. Lee, and E. J. Weinberg, Phys. Rev. D **42**, 3488 (1990).
[37] D. Bazeia and G. Lozano, Phys. Rev. D **44**, 3348 (1991).
[38] P. K. Ghosh and S. K. Ghosh, Phys. Lett. B **366**, 199 (1996).
[39] M. Deshaies-Jacques and R. MacKenzie, Phys. Rev. D **74**, 025006 (2006).
[40] A. Yu. Loginov, Phys. Lett. B **777**, 340 (2018).
[41] A. Yu. Loginov and V. V. Gauzshtein, Phys. Rev. D **99**, 065011 (2019).
[42] A. Yu. Loginov and V. V. Gauzshtein, Eur. Phys. J. C **79**, 780 (2019).
[43] R. Friedberg, T. D. Lee, and A. Sirlin, Nucl. Phys. **B115**, 1 (1976).
[44] R. Friedberg, T. D. Lee, and A. Sirlin, Nucl. Phys. **B115**, 32 (1976).